EurJIC
European Journal of Inorganic Chemistry

Full Papers
doi.org/10.1002/ejic.202100186

Chemistry Europe
European Chemical Societies Publishing

Special Issue

Dinuclear Organotin Building Blocks and their Conversion into a Tetranuclear Macrocycle Containing Sn–O–Sn Linkages

Gelen Gómez-Jaimes,[a, b, c] Irán Rojas León,[a, e] Rodolfo Martínez Romero,[a] Hiram I. Beltrán,*[c] Braulio Rodríguez-Molina,[d] Wolf Hiller,*[e] Klaus Jurkschat,*[e] Irán F. Hernández,[f] and Herbert Höpfl*[a]

Six dinuclear organotin building blocks of general composition RR′R″SnCH$_2$Si(CH$_3$)$_2$–biphenyl–Si(CH$_3$)$_2$CH$_2$SnR″R′R, in which the tin atoms are separated by a *p*,*p*′-biphenylene bridge and carry different substituents [**BD1** with R, R′ = CH$_2$Si(CH$_3$)$_3$, R″ = Ph; **BD2** with R, R′ = CH$_2$Si(CH$_3$)$_3$, R″ = Cl; **BD3**, with R, R′ = CH$_2$Si(CH$_3$)$_3$, R″ = I; **BD4** with R = CH$_2$Si(CH$_3$)$_2$(C$_5$H$_4$FeCp), R′, R″ = Ph; **BD5** with R = CH$_2$Si(CH$_3$)$_2$(C$_5$H$_4$FeCp), R′ = Ph, R″ = Cl; **BD6** with R = CH$_2$Si(CH$_3$)$_2$(C$_5$H$_4$FeCp), R′ = Ph, R″ = I], were synthesized and characterized by spectroscopic and spectrometric methods. Furthermore, the crystal and molecular structures of **BD2** were determined by single-crystal X-ray diffraction (SCXRD) analysis, revealing the formation of molecular strands through intermolecular Cl→Sn contacts. The 1D coordination polymer [**BD2**]$_n$ comprises macrocyclic rings of composition [**BD2**]$_2$ that motivated the generation of a related molecular macrocyclic structure by reaction of **BD2** with silver (I) oxide in a 2:2 stoichiometry. The [2 + 2] macrocyclization yielded the 30-membered tetra-nuclear ring structure **M1**, *viz.*, {[R$_2$SnCH$_2$Si(CH$_3$)$_2$–biphenyl–(CH$_3$)$_2$SiCH$_2$SnR$_2$](*μ*-O)}$_2$, in which two **BD2** dinuclear building blocks are linked through two covalent Sn–O–Sn moieties. Examination by DFT calculations at the B3LYP/def2svp and B3LYP/6-31G*(C,H,O,Si)/LanL2DZ(Sn) levels of theory gave energy minima for molecular conformers of **M1** carrying the Sn–O–Sn and *p*,*p*′-biphenylene bridges in *syn*- or *anti*-orientation.

[a] G. Gómez-Jaimes, Dr. I. Rojas León, R. Martínez Romero, Prof. Dr. H. Höpfl
Centro de Investigaciones Químicas, Instituto de Investigación en Ciencias Básicas y Aplicadas,
Universidad Autónoma del Estado de Morelos,
Av. Universidad 1001, Cuernavaca 62209, Morelos, México
E-mail: hhopfl@uaem.mx
[b] G. Gómez-Jaimes
Posgrado en Ciencias Naturales e Ingeniería,
Universidad Autónoma Metropolitana Cuajimalpa,
Ciudad de México 05300, México
[c] G. Gómez-Jaimes, Prof. Dr. H. I. Beltrán
Departamento de Ciencias Básicas, DCBI,
Universidad Autónoma Metropolitana Azcapotzalco,
Ciudad de México 02200, México
E-mail: hibc@azc.uam.mx
[d] Prof. Dr. B. Rodríguez-Molina
Instituto de Química,
Universidad Nacional Autónoma de México,
Ciudad de México 04510, México
[e] Dr. I. Rojas León, Prof. Dr. W. Hiller, Prof. Dr. K. Jurkschat
Fakultät für Chemie und Chemische Biologie,
Technische Universität Dortmund,
Dortmund 44221, Germany
E-mail: wolf.hiller@tu-dortmund.de
klaus.jurkschat@tu-dortmund.de
[f] Dr. I. F. Hernández
Centro Universitario de Tonalá, Universidad de Guadalajara,
Av. Nuevo Periférico 555, Ejido San José Tatepozco, Tonalá 45425, Jalisco, México

Supporting information for this article is available on the WWW under https://doi.org/10.1002/ejic.202100186

Special Issue

Part of the "Inorganic Chemistry in Latin America" Special Collection.

Introduction

Organotin (IV) compounds of composition R$_{4-n}$SnX$_n$ (with n = 0–3) are characterized by the presence of one or more covalent Sn–C bonds and are classified as mono-, di-, tri-, and tetra-organotin derivatives depending on the number of C-bound substituents. Despite being organometallic reagents, organotin compounds can be handled under non-inert conditions.[1] For the formation of tin–carbon bonds, the use of Grignard reagents is still a key strategy.[2] Organotin compounds carrying a single or two different organic substituents are quite common;[3] meanwhile, specimens carrying a larger number of diverse organic substituents are less explored. Among others, the research groups of Wardell and Gielen reported on tetra-organotin compounds of the R$_2$R^{1}R^{2}Sn and R^{1}R^{2}R^{3}R^{4}Sn types.[4,5]

The Sn–X bond in organotin compounds shows considerable ionic character, with X being an anionic moiety such as a halide, oxide, hydroxide, sulfide, carboxylate, dithiocarbamate, among others, of which particularly halides are used for further functionalization in subsequent reactions.[6] Organotin halides are prepared with high yields and purity by selective cleavage of tin–carbon bonds through reaction with elemental dihalogens (Cl$_2$, Br$_2$ or I$_2$) or treatment with hydrogen halides.[7]

Depending on the identity and number of substituents bound to the tin atom(s) in organotin compounds with diverse inorganic and organic ligands, the formation of specific and frequently complex molecular architectures is accomplished,[8,9] including metalla-macrocycles,[10–13] cage-type assemblies[14–18] and metal-organic frameworks (MOFs).[19–23] Changes of the

substitution pattern at the tin atoms modify the Lewis acidity and steric hindrance, which can be an important requisite for the successful formation of macrocyclic or cage-type structures.[11,24–27] Being Lewis acids, four-coordinate tin compounds count on the possibility of coordination number increase, enabling linkages with other compounds, e.g. solvent or guest molecules.[28] Because of these attributes, organotin compounds with interesting properties concerning the catalysis of transesterification and C–C coupling reactions,[29–30] anion and molecular recognition,[31–35] materials chemistry,[36–38] or biological activity[39–42] have been developed.

In the context of metalla-macrocyclic and supramolecular chemistry involving the element tin, generally mononuclear organotin compounds are combined with di- or oligotopic inorganic or organic ligands.[43–51] Although diverse di- and oligonuclear organotin specimens are known for more than 80 years (!) and easily accessible,[52] their employment for the assembly of macrocyclic and cage-type molecular architectures remains still underdeveloped. Recently, promising results have been achieved starting either from tin chalcogenide clusters[16,18,53–54] or di- or oligonuclear building blocks (tectons)[55–56] containing organic spacers serving as connectors between the metal atoms.[10,11,13,14,17,18,57–64] An elegant general synthetic methodology towards di-, tri- and tetranuclear building blocks, in which the tin atoms are interconnected by an aliphatic or aromatic organic spacer, consists in the functionalization of organohalides with $-Si(CH_3)_2CH_2Cl$ substituents followed by derivatization with organotin moieties.[24,59,65–66] Interconnection of such organotin tectons through di- or oligotopic ligands such as carboxylates, dithiocarbamates, phosphates, etc., constitutes a pathway to a plethora of metalla-supramolecular assemblies.[65–66]

In continuation of previous works,[11,24,59,65–67] herein we report on the formation of two di-nuclear organotin compounds carrying voluminous organic substituents at the metal atoms that were then functionalized with a Sn–X bond (X = Cl, I). In addition, the potential for the formation of a novel class of tetra-nuclear macrocyclic structures through linkage of the halogenated building blocks by Sn–O–Sn fusion[11,68] was explored.

Results and Discussion

Synthetic procedure for the preparation of BD1–BD6

The bis(chloromethyldimethylsilyl)-substituted precursor (*p*-$ClCH_2Me_2SiC_6H_4)_2$ (**PRE**) is obtained in good yields by reaction of the Grignard reagent (*p*-$BrMgC_6H_4)_2$ with (chloromethyl) dimethylchlorosilane, $ClMe_2SiCH_2Cl$. Subsequently, the Grignard reagent (*p*-$ClMgCH_2Me_2SiC_6H_4)_2$ reacts with $Ph[(CH_3)_3SiCH_2]_2SnI$ and $Ph_2[CpFe(C_5H_4Si(CH_3)_2CH_2)]SnI$ giving the spacer-bridged bis (tetraorganotin) compounds **BD1** and **BD4**, respectively, in good yields (Scheme 1). The subsequent conversion of Sn-phenyl groups into Sn–X (X = Cl, I) functions is frequently a major challenge due to multiple Sn–C bond rupture issues upon treatment with hydrogen chloride or iodine.[7] However, our previous studies have shown that the reaction proceeds straightforward when $-Si(CH_3)_2CH_2-$ segments are introduced between the Sn-phenyl and the organic spacer groups in di- and oligo-nuclear organotin substrates.[24,59,65–66] Accordingly, treatment of **BD1** and **BD4** with hydrogen chloride and elemental iodine yielded the halogen-substituted analogues **BD2**, **BD3**, **BD5** and **BD6**, respectively, in almost quantitative yield (Scheme 1).

The synthetic methodology illustrated in Scheme 1 accomplishes our previous reports on the related dinuclear tri- and diphenyl-tin tectons **BD7**–**BD9**,[65,66] thus constituting an elegant route to diverse bis-functionalized organotin compounds carrying aliphatic, aromatic and ferrocenyl-substituents. In this context, it is also important to note that compounds **BD5** and **BD6** carry four different substituents at each tin atom converting the latter into stereogenic centers. As already mentioned in the introduction, reports on triorganotin halides of composition $R^1R^2R^3SnX$ are still scarce.

The dinuclear organotin compounds **BD1**–**BD6** were thoroughly characterized by elemental analysis, IR and NMR spectroscopy and mass spectrometry (Figures S1–S34, and Tables S1–S4, ESI). Moreover, single-crystals suitable for X-ray diffraction analysis were obtained for **BD2** after slow solvent evaporation of a solution in $CHCl_3$/MeOH (4:1, *v*/*v*).

NMR spectroscopic characterization of BD1–BD6

Complete assignment of the ^1H and ^{13}C NMR signals of compounds **BD1**–**BD6** was achieved by two-dimensional COSY, HSQC and HMBC NMR experiments (Figures S1–S32, ESI) and comparison with the previously reported analogues **BD7**–**BD9**.[65,66] The NMR spectroscopic analysis reveals characteristic features for the two product series, which are described in what follows in comparative manner. Figure 1a illustrates the aliphatic regions of the ^1H and ^{13}C NMR spectra of the bis [(trimethylsilyl)methyl]stannyl derivatives **BD1**–**BD3**, showing characteristic changes upon replacement of the tin-bound phenyl group by a halogen substituent (for complete NMR spectra, see Figures S1–S9 and S13–S16, ESI). In the aliphatic region, each ^1H NMR spectrum exhibits four signals with relative intensities of 1:2:3:9 for the $SiCH_2$ protons H2 and H3 and the $SiCH_3$ protons H1 and H4, respectively. As expected, the signals for the protons belonging to the biphenyl–$Si(CH_3)_2CH_2-$ groups (H1 and H2) are shifted towards higher frequencies than the

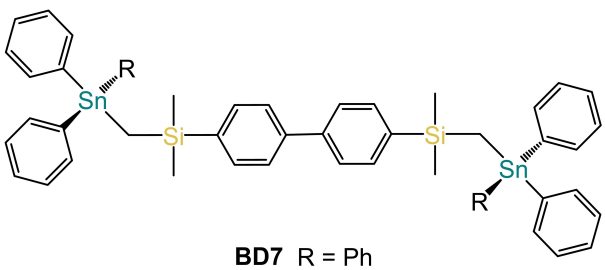

BD7 R = Ph
BD8 R = Cl
BD9 R = I

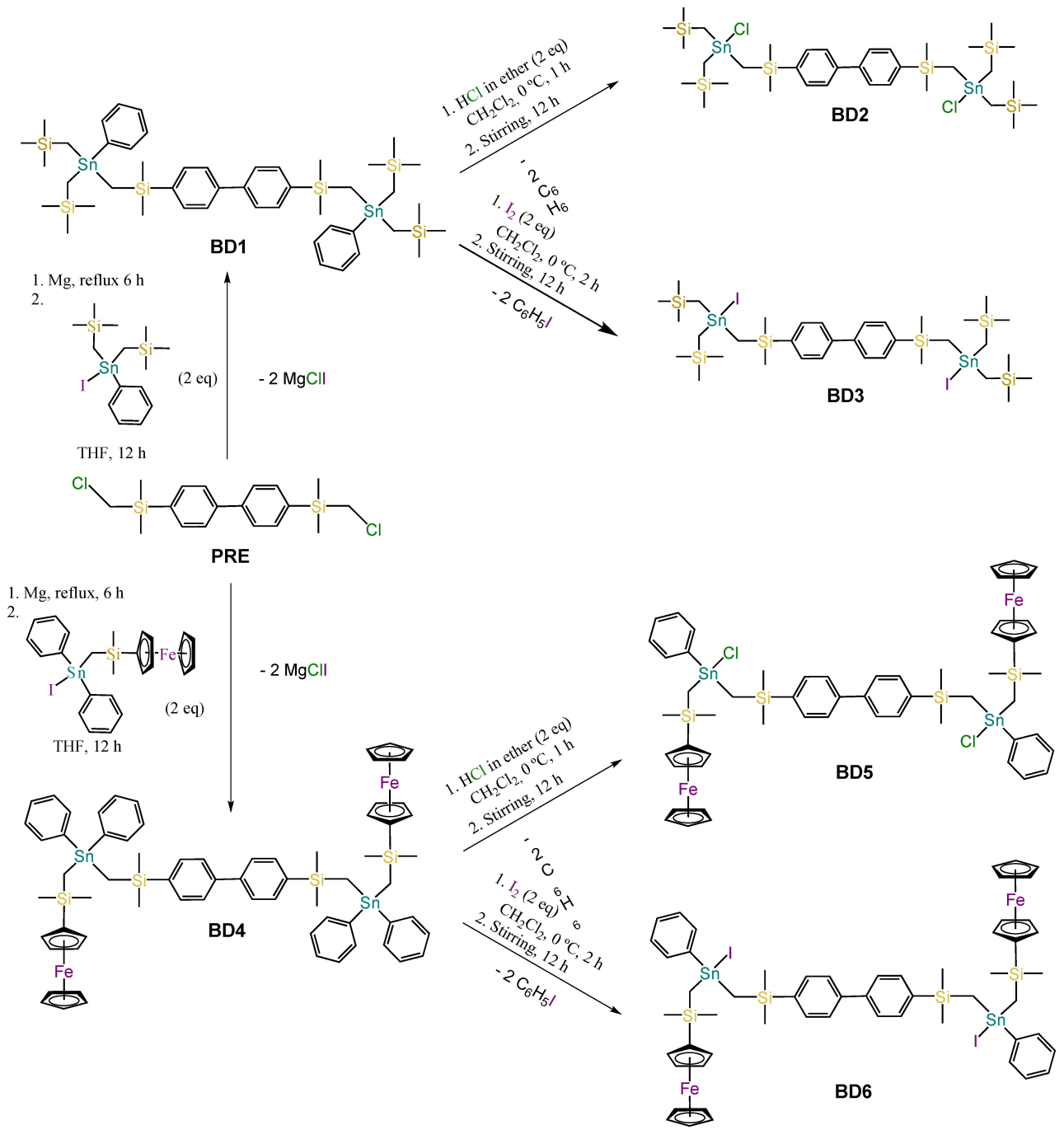

Scheme 1. Synthetic procedures for the functionalization of **PRE** to obtain **BD1**–**BD6**.

resonances for the $-CH_2Si(CH_3)_3$ protons (H3 and H4). The replacement of the phenyl groups by halogen substituents induces a significant low-field shift of the ^{1}H NMR signals, which is larger for the iodine-substituted derivative **BD3** than for the chlorine-substituted analogue **BD2**. The largest chemical shift difference occurs for H2 followed by H3, H1 and H4 (Table 1).

In the ^{13}C NMR spectrum of **BD1** (R = Ph), the Si–methylene carbon atoms are shielded compared to Me_4Si, indicating an anisotropic shielding effect from the tin atoms. Upon halogenation, these signals are shifted significantly to higher frequencies ($\Delta\delta \approx 8$–9 ppm, Table 1). As seen from Figure 1a, in relation to **BD1** the chemical shift difference is now slightly smaller for the iodine-substituted derivative **BD3** than for the chlorine-substituted analogue **BD2**.

The ^{119}Sn NMR spectra for **BD1**–**BD3** measured in $CDCl_3$ gave signals at $\delta = -14$, 173 and 39 ppm, respectively, corresponding to organotin compounds having tetrahedral metal geometries.[69] For comparison, the chemical shifts of Me_4Sn, Me_3SnCl and Me_3SnI are 0.0, +164 and +39 ppm, respectively.[69] Accordingly, the ^{29}Si NMR spectra revealed non-

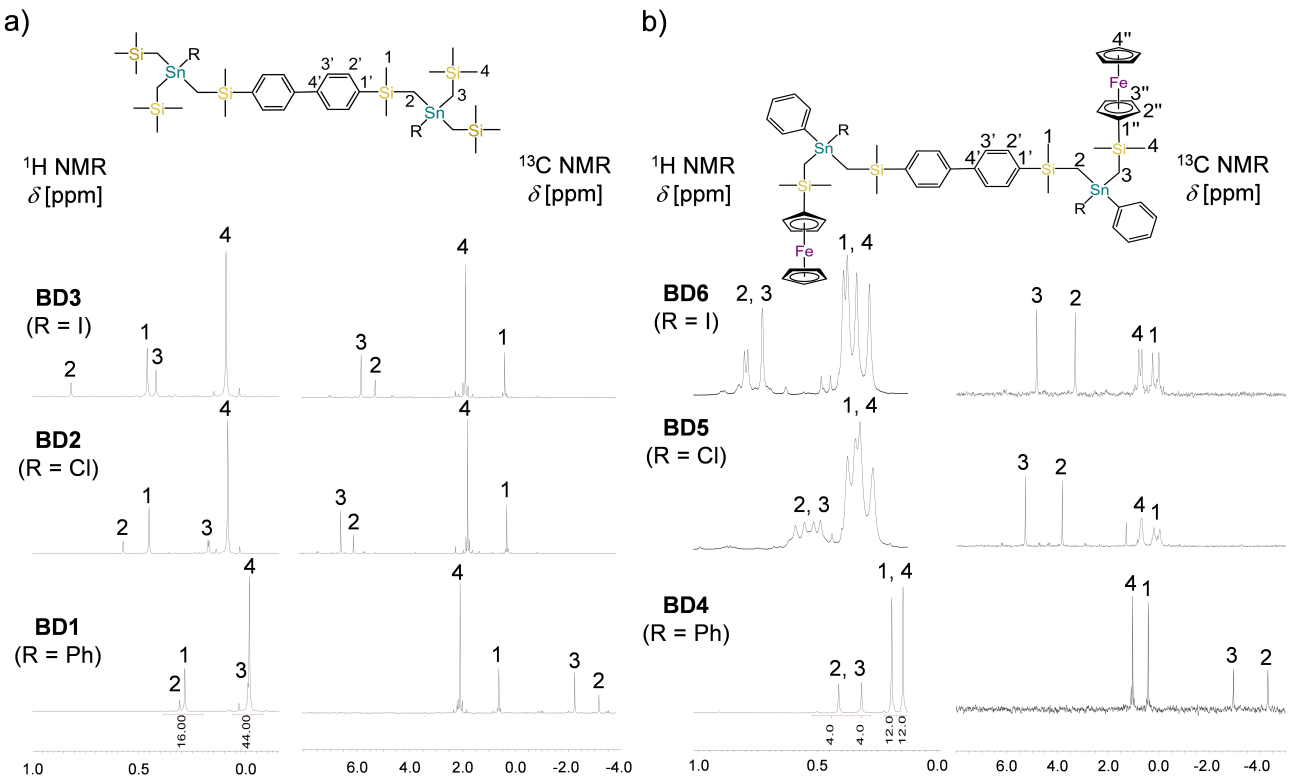

Figure 1. Comparison of the aliphatic range in the ^{1}H and ^{13}C NMR spectra for a) **BD1**–**BD3** and b) **BD4**–**BD6**.

Table 1. Comparison of selected ^{1}H, ^{13}C, ^{29}Si and ^{119}Sn NMR spectroscopic data for **BD1**–**BD9** (ppm, $CDCl_3$).

	^{1}H				^{13}C				^{29}Si	^{119}Sn	Reference
	H1[a]	H2[b]	H3[b]	H4[a]	C1	C2	C3	C4			
BD1	0.30, s	0.32, s	0.00, s	−0.01, s	0.6	−3.1	−2.2	2.1	−2.0, 2.4	−14	this work
BD2	0.45, s	0.57, s	0.17, s	0.08, s	0.3	6.1	6.6	1.8	−2.6, 2.3	+173	this work
BD3	0.46, s	0.82, s	0.42, s	0.09, s	0.4	5.3	5.8	1.9	−2.1, 2.9	+39	
BD4	0.19, s	0.41, s	0.31, s	0.14, s	0.4	−4.3	−2.9	1.0	−1.8, −1.3	−51	this work
BD5	0.32, s	0.55, s	0.49, s	0.27, s	0.0	3.9	5.3	0.7	−2.5, −2.0	+98	this work
	0.37, s	0.59, s	0.52, s	0.34, s	0.3			0.8			
BD6	0.33, s	0.79, s	0.73, s	0.28, s	0.1	3.4	4.9	0.7	−2.0, −1.5	−13	this work
	0.39, s	0.81, s		0.37, s	0.3			0.9			
BD7	0.15, s	0.64, s	–	–	0.4	−5.3	–	–	−1.6	−90	[65]
BD8	0.41, s	1.01, s	–	–	0.1	2.4	–	–	−2.2	+26	[65]
BD9	0.15, s	0.96, s	–	–	0.2	2.7	–	–	−1.8	−64	[65]

[a] Data might be interchanged in the case of **BD5**. [b] Data might be interchanged in the case of **BD6**.

equivalent silicon nuclei with signals in the range of −2.6 to −2.0 ppm for the biphenyl–*Si*$(CH_3)_2CH_2$– and in the range of 2.3 to 2.9 ppm for the –CH_2*Si*$(CH_3)_3$ silicon atoms. The shielding effect on the silicon atom attached to the aromatic biphenyl connector is confirmed by comparison with the ^{29}Si NMR spectra of the CpFe[C_5H_4Si$(CH_3)_2CH_2$]-substituted analogues **BD4**–**BD6**, for which the chemical shifts are all negative (−2.5 to −1.3 ppm) in comparison to Me_4Si. The same is true for compounds **BD7**–**BD9** (Table 1).[65]

For **BD1**–**BD3**, the aromatic regions in the ^{1}H NMR spectra show a characteristic AB-system at approximately δ = 7.5–7.6 ppm for the C*H* hydrogen atoms of the biphenyl spacer (Tables S1–S2, ESI).

At first sight, the ^{1}H and ^{13}C NMR spectra of the tetraorganotin compounds **BD1** and **BD4** are similar; however, a closer inspection shows some important differences, which illustrate some particularities in the electronic features of the series. In the ^{1}H NMR spectrum, the Si–methyl groups (H1) attached to the biphenyl connector in **BD4** are more shielded than in **BD1**, giving a chemical shift similar to the SiCH_3 protons (H4) close to the ferrocenyl-substituent. Since the high-field shift in **BD4** affects only the methyl protons H1 and not the methylene protons H2, the change can be attributed to an anisotropic shielding effect of one of the Sn–phenyl groups. This is also somewhat illustrated by the molecular structures of the recently reported related compounds **BD7**–**BD9**, which are

all indicative of an intramolecular (Si)CH_3···π contact.[66] Moreover, comparison of the ^{13}C NMR spectra of **BD1** and **BD4** shows an enhanced shielding effect for all aliphatic ^{13}C NMR signals in **BD4** (Figure 1b, Table 1).

The tin atoms in the triorganotin halide derivatives **BD5** and **BD6** are stereogenic centers making the SiCH_2 methylene and the SiCH_3 methyl protons diastereotopic. The ^{1}H and ^{13}C NMR spectra reflect this as they exhibit splitting of the signals in the aliphatic region corresponding to hydrogen and carbon atoms in chemically non-equivalent positions (H1, H2, H3, H4, C1 and C4 in Figure 1b). Of these, the only signal without apparent splitting is that originated from the methylene proton H3 in compound **BD6**. Due to their location at the molecule periphery, the chemical shift differences for the ^{1}H NMR signals are larger for the SiCH_3 protons (H1 and H4) than for the SiCH_2 protons H2 and H3. The larger diastereotopic effect for the methylene protons in **BD5** compared to **BD6** can be attributed to the smaller distance of the Sn–Cl bond, bringing the chlorine substituent closer to the H2/H2′ and H3/H3′ nuclei (Figure 1b, Table 1). Although the general tendencies for the chemical shift variations in the aliphatic region of the series **BD4**–**BD6** are similar to those observed for **BD1**–**BD3**, for the SiCH_2 protons most of the ^{1}H NMR signals in **BD4**–**BD6** are shifted to higher frequencies, in accordance with the negative inductive effect of phenyl substituents (Table 1). However, the corresponding carbon and tin nuclei are shielded, reflecting the known anisotropic shielding effect of phenyl groups on tin atoms.[69] The chemical shift differences for the ^{119}Sn NMR signals between the **BD1**–**BD3** and **BD4**–**BD6** series are in the range of $\Delta\delta = 37$–75 ppm (Table 1). These observations are in line with the tendencies observed for the triphenyl- and diphenyl-substituted analogues **BD7**–**BD9**, for which the shielding effects described above are still more enhanced.[65] Interestingly, for the ^{119}Sn NMR signals the chemical shift differences between the **BD4**–**BD6** and **BD7**–**BD9** series are very similar ($\Delta\delta = 49$–72 ppm) to those detected in the comparison of the **BD1**–**BD3** and **BD4**–**BD6** series (Table 1).

Analysis of the molecular and supramolecular structure of BD2 by SCXRD

Single crystals of **BD2** were obtained from its solution in $CHCl_3$/MeOH. **BD2** crystallized in the monoclinic space group *C*2/c. Figure 2 shows the molecular structure, Table 2 contains selected interatomic distances and angles, and Table S7 (ESI) summarizes the crystal and refinement data.

The molecular structure of **BD2** has crystallographic 2-symmetry. In relation to the central –$CH_2Si(CH_3)_2$–biphenyl–Si-$(CH_3)_2CH_2$– fragment, the voluminous –Sn[$CH_2Si(CH_3)_3$]$_2$Cl substituents point into opposite directions, giving an overall *anti*-conformation, which is indicated by the Sn···Si$(CH_3)_2$···Si$(CH_3)_2$···Sn dihedral angle of 158.4°. Although in **BD2** the chloro-bis[(trimethylsilyl)methyl]stannyl moieties are oriented in opposite directions with respect to the biphenyl connector, the Sn[$CH_2Si(CH_3)_3$]$_2$Cl groups are twisted around the Sn–CH_2[$Si(CH_3)_2C_{biph}$] bond with the Sn–Cl bonds pointing into the same direction (mutual *syn*-orientation). The C1–Si1–C7–Sn1 torsion angle is 41.8(9)° (Table 2). The C_6H_4-groups in the *p,p*′-biphenylene spacer are significantly out-of-plane rotated, as indicated by the twist of 43.3° formed between the mean planes, to mitigate the H···H repulsion in the central region of the connector. The molecular twofold rotation axis is perpendicular to the central C_{biph}–C_{biph} (C4–C4′) bond and passes in between the *ortho*-hydrogen atoms. The Sn–Cl bonds are almost parallel to the 2-axis.

Table 2. Selected interatomic distances [Å], angles and torsion angles [°] for compound **BD2**.[a]

Distances			
Sn1–C7	2.108(14)	Sn1–C14	2.139(19)
Sn1–C10	2.155(16)		
Sn1–Cl1	2.350(4)	Sn1···Cl1^{ii}	4.094(4)
Sn1···Sn1^{i}	12.404(2)	Sn1···Sn1^{ii}	6.412(1)
Si1···Si1^{i}	10.880(7)	Cl1···Cl1^{i}	12.400(8)
Angles			
Sn1–C7–Si1	121.4(6)	Sn1–C10A–Si2A	120.5(14)
Sn1–C14A–Si3A	120.2(16)		
Cl1–Sn1–C7	104.5(3)	C1–Si1–C7	110.3(6)
Cl1–Sn1–C10A	106.2(10)	C1–Si1–C8	109.4(7)
Cl1–Sn1–C14A	109.2(11)	C1–Si1–C9	109.7(7)
C7–Sn1–C10A	108.8(8)	C7–Si1–C8	108.8(6)
C10A–Sn1–C14A	118.5(12)	C7–Si1–C9	110.0(7)
C7–Sn1–C14A	108.7(12)	C8–Si1–C9	108.6(7)
Sn1–Cl1···Sn1^{iii}	168.1(2)	Cl1···Sn1–Cl1^{iii}	168.1(1)
Torsion angles			
Si1–C7–Sn1–Cl1	+47.9(7)	Sn1–C7–Si1–C1	+41.8(9)
Si1–C7–Sn1–C10A	−65(1)	Si1–C7–Sn1–C14A	164(1)

[a] Symmetry operators: (i) 1−x, y, 0.5−z; (ii) x, 1+y, z; (ii) x, −1+y, z

The interatomic distances between the tin atoms and their substituents are as expected, with the Sn–C distances ranging from 2.108(14) to 2.155(16) Å. The Sn–Cl distance is 2.350(4) Å. Due to the large steric hindrance of the –$CH_2Si(CH_3)_3$ substituents, the three Si–CH_2–Sn angles are significantly enlarged, with values ranging from 120.2(16) to 121.4(6)°. In addition, the small Cl–Sn–C angles of 104.5(3), 106.2(10) and 109.2(11)° are indicative of a slight distortion towards a trigonal-bipyramidal environment of the tin atom. The distortion originates from a rather weak intermolecular Sn–Cl→Sn interaction with a distance of 4.094(4) Å that is similar to the sum of the Van der Waals radii for tin and chlorine (4.05 Å).[70] Such Cl→Sn interactions were previously observed also in the crystal structures of *t*BuC_6H_4Sn$(CH_3)_2$Cl,[71] 2-$(Me_2NCH_2)C_6H_4$Sn(*n*Bu)Cl_2,[72] [Ph_2ClSn–CH_2–Y–CH_2–SnClPh$_2$] with Y = –C_2H_4– and –C_6H_4–,[73] among others.[74]

The intermolecular Sn–Cl→Sn contacts among adjacent molecules in the crystal structure generate 1D molecular strands [**BD2**]$_n$ running parallel to [0 1 0] (Figure 2b). Because of the mutual *syn*-orientation of the Sn–Cl bonds, the coordination polymer is composed of large 30-membered tetra-nuclear macrocyclic rings. The perspective view of the macrocyclic [**BD2**]$_2$ aggregate given in Figure 2b reveals intra- and intermolecular Sn···Sn distances of 12.404(2) and 6.412(1) Å, respectively. The Cl→Sn–Cl interatomic angle of 168.1(1)°

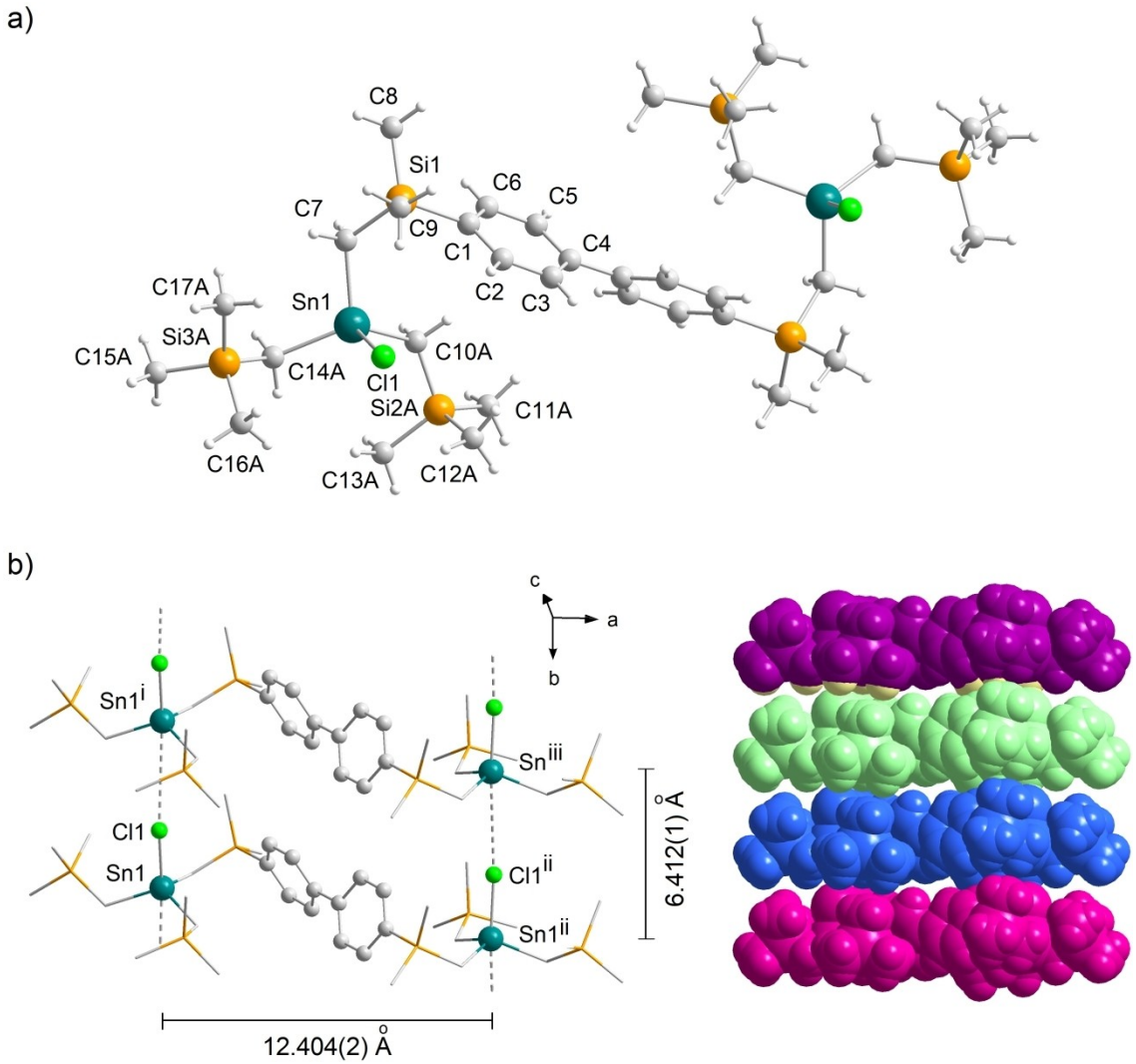

Figure 2. Fragments of the crystal structure of compound **BD2**, showing a) the molecular structure of the dinuclear building block and the coordination environment of the tin atoms, and, (b) the [1 + 1] macrocyclic assembly within the molecular strands formed through Cl→Sn contacts together with a spacefilling view of the 1D coordination polymer $[\mathbf{BD2}]_n$. Symmetry operators: (i) x, −1 + y, z; (ii) 1−x, y, 0.5−z; (iii) 1-x, −1 + y, 0.5−z.

approaches 180°, as expected for a distorted trigonal-bipyramidal polyhedron. Similar arrangements have been reported previously for compounds $[Ph_2ClSnCH_2–Y–CH_2SnClPh_2]$ with Y = $–C_2H_4–$ and $–C_6H_4–$.[73]

In solution, the weak intermolecular Cl→Sn contacts found in the solid-state structure are disrupted. This is deduced from the ^{119}Sn NMR chemical shift typical for a four-coordinate triorganotin chloride R_3SnCl (δ = 173 ppm, *vide supra*) and was further confirmed by diffusion-ordered spectroscopy (DOSY) in C_6D_6. DOSY experiments enable the measurement of the diffusion coefficient of a chemical species in solution.[75] The diffusion coefficient depends on the molecular weight and volume, which can be, therefore, established. The ^{1}H-DOSY NMR spectrum of **BD2** revealed a single species with a diffusion coefficient of $D = 5.47 \cdot 10^{-10}$ m^2 s^{-1} (Figure S11, ESI) that according to Morris' procedure[76] corresponds to a molecular weight of MW_{calc} = 1088 g·mol^{-1}. The molecular weight corresponding to the elemental composition of **BD2** in monomeric form is 953.75 g·mol^{-1}. A monomeric composition of **BD2** was also found in the mass spectrometric analysis using the FAB technique in the positive ionization mode. The resulting mass spectrum gave a well-defined and high-intensity mass cluster at *m/z* = 917 (88%) corresponding to the $[M–Cl]^+$ ion (Figure S12, ESI). The loss of halide ions coordinated to tin atoms is commonly observed in mass spectra of tin compounds and can be attributed to the elimination of HX from the $[M+H]^+$ ion formed upon protonation by the medium used for the experiment.[77]

Preparation and characterization of the [2 + 2] tetra-nuclear macrocyclic assembly M1

Previously, building blocks **BD8** and **BD9** have been successfully employed for the [1 + 1] assembly of di-nuclear 21- and 22-membered organotin macrocycles using the potassium salts of

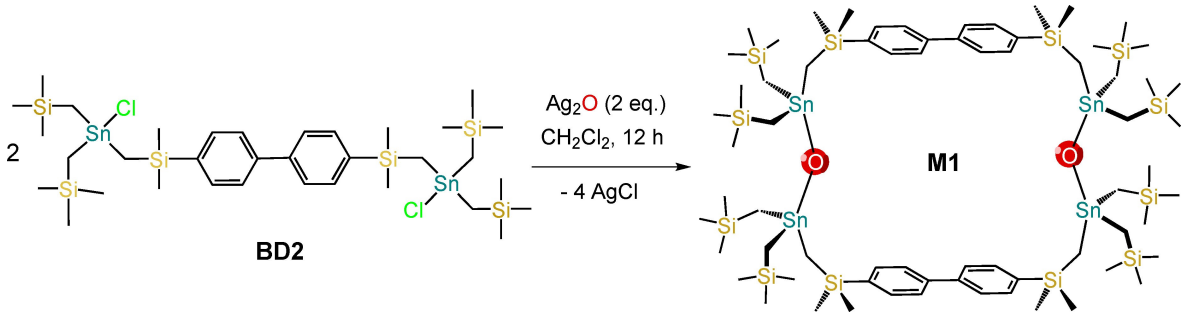

Scheme 2. Preparation of the [2 + 2] macrocycle **M1** starting from building block **BD2**.

terephthalate, 2,5-pyridinedicarboxylate, 3,5-pyridinedicarboxylate and piperazine-bis-dithiocarbamate, respectively, as ligands.[66] In order to generate larger macrocycles, herein we explored the combination of building block **BD2** with the small oxide anion O^{2-}, which due to the large biphenyl connector is not able to facilitate [1 + 1] ring closure, inducing the formation of a [2 + 2] or larger assembly. Reaction of **BD2** with silver (I) oxide, Ag_2O, in CH_2Cl_2 gave the 30-membered tetra-nuclear organotin macrocycle **M1** in good yield (Scheme 2). **M1** is soluble in solvents such as C_6H_6, CH_2Cl_2, $CHCl_3$ and THF. The macrocyclic structure of **M1** resembles the [1 + 1] aggregate described in the crystal structure analysis section of **BD2** (Figure 2b), resulting from replacement of the μ-Cl atoms in [**BD2**]$_2$ by μ-O bridges.

The number, multiplicity and integration of the signals in the ^{1}H, ^{13}C, ^{29}Si and ^{119}Sn NMR spectra (see Figures S35–S39 and Tables S5–S6, ESI) for the product indicate a highly symmetric and conformationally flexible molecular structure, in agreement with the expected macrocyclic compound (**M1**). Figure 3 shows a comparison of the ^{1}H and ^{119}Sn NMR spectra of **M1** and building block **BD2**, illustrating evident chemical shift differences. Table 3 summarizes additional NMR data. Upon formation of the Sn–O–Sn bridges, the ^{1}H NMR resonances belonging to the Sn–CH_2–Si methylene protons are shifted to lower frequencies ($\Delta\delta$ = 0.22 and 0.18 ppm for H2 and H3, respectively). Accordingly, the corresponding carbon nuclei are upfield-shifted with differences of $\Delta\delta$ = 2.2 (C2) and 2.0 (C3) ppm. The ^{119}Sn NMR signal for **M1** is upfield shifted by $\Delta\delta$ = 40 ppm compared to **BD2**. Similar trends in the ^{119}Sn NMR spectra were previously found for the Me_3SnCl)/$Me_3SnOSnMe_3$ (δ = 164/109.5 ppm) and Et_3SnCl)/$Et_3SnOSnEt_3$ (δ = 155/87 ppm) pairs of molecules.[69]

A DOSY experiment performed in C_6D_6 evidenced the formation of a single macrocyclic species (**M1**) (Figure S41, ESI). The diffusion coefficient of $D = 4.83 \cdot 10^{-10}$ m^2 s^{-1} and calculated molecular weight based on Morris' procedure[76] (MW_{calc} = 1798 g·mol^{-1}) are in excellent agreement with the expected data. Interestingly, the diffusion coefficient of macrocyclic **M1** is similar to the value reported for the 22-membered di-nuclear macrocycle isolated from the reaction of **BD8** and **BD9** with the potassium salt of piperazine-bis-dithiocarbamate,[66] indicating a similar hydrodynamic volume in solution. Because of this, it can be assumed that **M1** lacks a solvent-accessible cavity and is folded in solution (*vide infra*). The diffusion constant of **M1** is also comparable to the value reported by Cohen for a tetra-

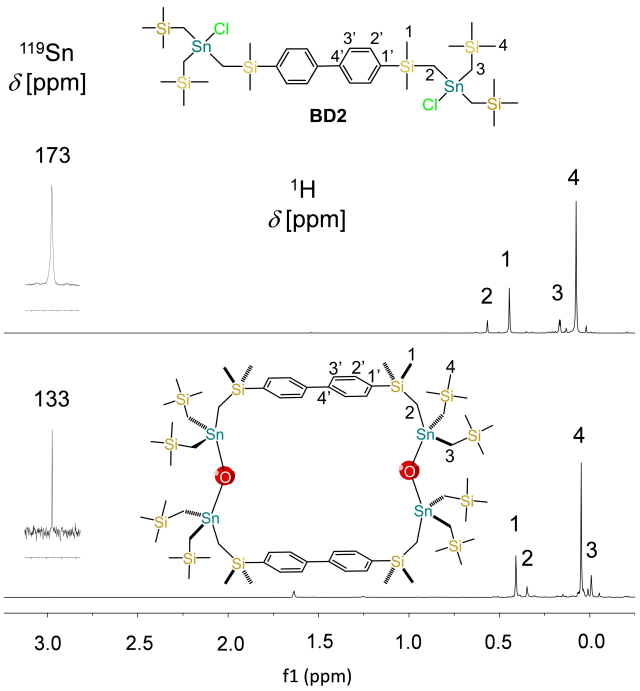

Figure 3. Comparison of the ^{1}H and ^{119}Sn NMR spectra of building block **BD2** and macrocycle **M1**.

Table 3. Comparison of selected ^{1}H, ^{13}C, ^{29}Si and ^{119}Sn NMR spectroscopic data for **BD2** and **M1** (ppm, $CDCl_3$).

	^{1}H				^{13}C				^{29}Si	^{119}Sn
	H1	H2	H3	H4	C1	C2	C3	C4		
BD2	0.45, s	0.57, s	0.17, s	0.08, s	0.3	6.1	6.6	1.8	−2.6, 2.3	+173
M1	0.41, s	0.35, s	−0.01, s	0.05, s	0.5	3.9	4.6	1.9	−2.9, 1.6	+133

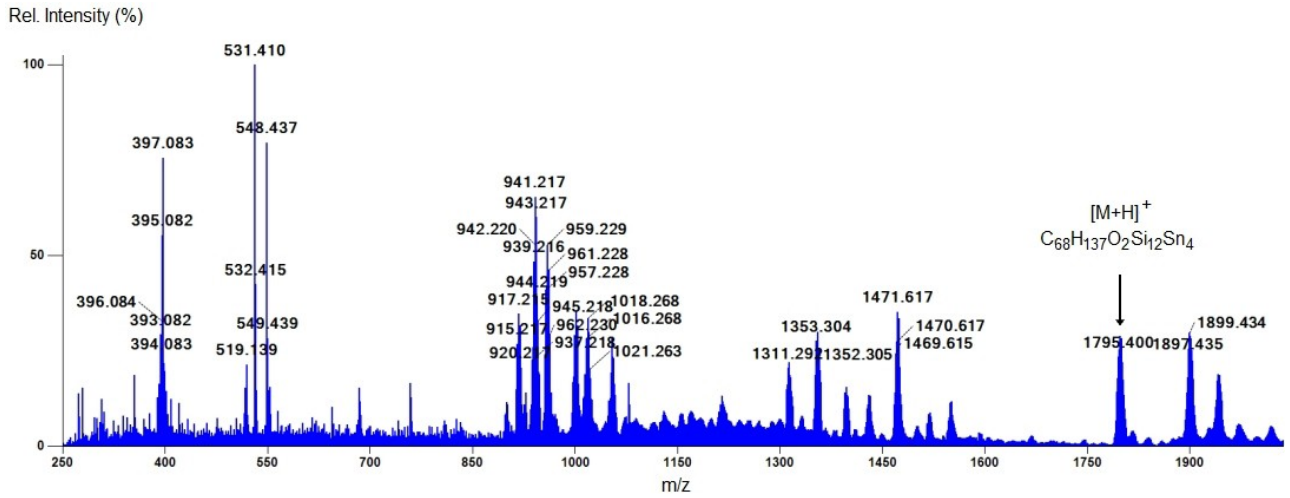

Figure 4. Mass spectrum of **M1** (in $CHCl_3$–MeOH, 5:1, *v/v*) recorded using the paperspray technique, showing the mass cluster for $[M+H]^+$ (relative abundance: 29%). **Note**: Mass clusters at $m/z \geq 1900$ are attributed to reactions with the solvent, since these are not observed in the DART experiment (see Figure S42, ESI).

urea calix[4]arene of similar size ($MW = 1160\ g \cdot mol^{-1}$, $D = 4.6 \cdot 10^{-10}\ m^2\ s^{-1}$; solvent C_6D_6 with 3% DMSO).[78]

The composition of macrocycle **M1** was further confirmed by mass spectrometric studies, using the ESI, paperspray and DART techniques. Of these, the paperspray method gave the strongest peak intensity (29%) for the mass cluster of the molecular ion (Figure 4). The elemental composition was determined by means of the abundant isotope approach,[79] revealing excellent matching of the experimental and simulated pattern for 30 isotopes, with an rms mass error of 0.7 mmu. Figure S42 shows the mass spectrum of **M1** recorded with the DART technique, revealing again a mass cluster for the molecular ion. Although the relative abundance in this case is much lower (≈2%), with this technique less additional products due to interaction/reaction with the medium are observed (compare regions close to $m/z = 1750$–2000 in Figure 4 and Figure S42).

Analysis of the molecular strain and possible conformations of M1 by DFT calculations

Attempts to obtain suitable crystals for SCXRD analysis of **M1** were unsuccessful; however, the molecular structure of **M1** could be successfully geometry-optimized in the gas phase by DFT calculations using the B3LYP functional[80,81] and the def2-svp (SB)[82] and 6–31G*/LanL2DZ (LB)[83,84] basis sets (SB and LB = small and large basis set, respectively)[85] implemented in the NWChem program suite.[86] These basis sets were employed previously in research dealing with computational calculations on organotin complexes, showing that they confidently reproduce the geometries of organotin compounds.[12,32,51,65,87–90]

Geometry optimizations were performed using two general minimization models, one for $\mathbf{M1}_{SYN}$ and another for $\mathbf{M1}_{ANTI}$, where the two connecting branches of the organic spacer $-CH_2Si(CH_3)_2$–biphenyl–$Si(CH_3)_2CH_2-$ to develop macrocycle **M1** are binding to the tin atoms from the same (*syn*) or opposite sides (*anti*), respectively (Scheme 3). At the same time, the –Sn–O–Sn– linkages are mutually *syn*- ($\mathbf{M1}_{SYN}$) or *anti*-oriented ($\mathbf{M1}_{ANTI}$).

$\mathbf{M1}_{ANTI}$ was developed from the crystal structure packing and conformation found in parent $[\mathbf{BD2}]_2$ (*vide supra*) and three potential energy minima were detected, named $\mathbf{M1\text{-}0}_{ANTI}$, $\mathbf{M1\text{-}1}_{ANTI}$ and $\mathbf{M1\text{-}2}_{ANTI}$, of which the latter was the most stable conformer and used for further comparisons. In the optimization of the *syn*-conformer, only a single minimum structure was found, $\mathbf{M1\text{-}3}_{SYN}$. Table 4 resumes the energy values obtained for $\mathbf{M1\text{-}0}_{ANTI}$, $\mathbf{M1\text{-}1}_{ANTI}$, $\mathbf{M1\text{-}2}_{ANTI}$ and $\mathbf{M1\text{-}3}_{SYN}$ after energy minimizations, employing the small and large basis sets described above. Of these, $\mathbf{M1\text{-}3}_{SYN}$ is the most stable conformer in the gas phase with an energetic stabilization of ΔE [kcal·mol^{-1}] = −2.32 (LB) or −1.95 (SB) in comparison to the lowest-energy *anti*-conformer $\mathbf{M1\text{-}2}_{ANTI}$.

Table 5 contains relevant geometrical details for the most stable conformers, $\mathbf{M1\text{-}2}_{ANTI}$ and $\mathbf{M1\text{-}3}_{SYN}$. The molecular structures are compared in Figure 5. The Sn–O and Sn–C interatomic distances [Å] in the calculated compounds are similar for the two stereoisomers, but there is a clear tendency

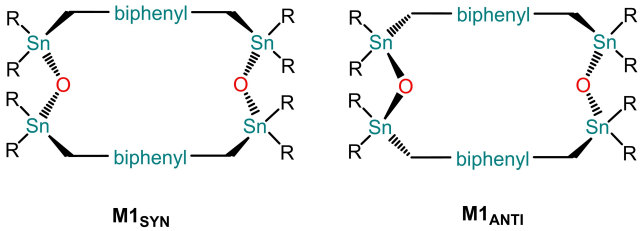

$\mathbf{M1}_{SYN}$ $\mathbf{M1}_{ANTI}$

Scheme 3. Illustration of the structural differences between the calculated conformers of $\mathbf{M1}_{SYN}$ and $\mathbf{M1}_{ANTI}$.

Table 4. Energies and relative energy differences determined by DFT computational studies for *syn*- and *anti*-conformers of **M1** at the B3LYP-6-31G*/(Sn)LanL2DZ and B3LYP/def2-svp levels of theory.[a]

Conformer	Energy [kcal·mol^{-1}]	ΔE [kcal·mol^{-1}]
M1-0$_{ANTI}$ LB	−3960539.158	0.000
M1-1$_{ANTI}$ LB	−3960539.613	−0.455
M1-2$_{ANTI}$ LB	−3960540.090	−0.932
M1-3$_{SYN}$ LB	−3960542.407	−3.249
M1-0$_{ANTI}$ SB	−4488295.569	0.000
M1-1$_{ANTI}$ SB	−4488295.967	−0.398
M1-2$_{ANTI}$ SB	−4488296.393	−0.824
M1-3$_{SYN}$ SB	−4488298.338	−2.769

[a] LB (large basis set): 6-31G*/(Sn)LanL2DZ; SB (small basis set): def2-svp.

for Sn–O and Sn–C distance enlargement with the small basis set, giving less strained structures. A comparison of the Sn–O distances calculated for **M1** using the large basis set (1.935–1.946 Å) with the SCXRD data reported for $(Ph_3Sn)_2O$[91] [i.e., 1.952(2) and 1.957(2) Å], $(Bn_3Sn)_2O$[92] [i.e., 1.919(1) Å], $(tBu_3Sn)_2O$[93] [i.e., 1.954(1) Å] and {[4-(FC_6H_4)Si$(CH_3)_2CH_2]_3Sn\}_2O$[94] [i.e., 1.960(3) Å] shows good agreement. The C–Sn–C angles in the range of 108.3–114.4/108.3–116.0° and 108.9–114.4/109.7–116.4° for **M1-3$_{SYN}$** (LB/SB) and **M1-2$_{ANTI}$** (LB/SB), respectively, are larger than the C–Sn–O angles [104.6–109.4/104.5–112.3° for **M1-3$_{SYN}$** (LB/SB); 104.4–109.5/103.4–108.4° for **M1-2$_{ANTI}$** (LB/SB)] (Table S8, ESI). Nevertheless, the values are typical for tetrahedral coordination geometries around tin atoms with sterically demanding substituents. On the contrary, the Sn–O–Sn angles are significantly increased [**M1-3$_{SYN}$**: 135.0/141.4° (LB) and 129.7/139.8° (SB); **M1-2$_{ANTI}$**: 146.2/135.3° (LB) and 140.4/131.0° (SB)], with values similar to those observed in the SCXRD structures of $(Ph_3Sn)_2O$[91] [i.e., 137.3(1)°] and {[4-(FC_6H_4)Si$(CH_3)_2CH_2]_3Sn\}_2O$[94] [i.e., 140.13(16)°]. However, in $(Bn_3Sn)_2O$[92] and $(tBu_3Sn)_2O$[93] the Sn–O–Sn angles are 180.0°, which has been attributed to low metal electronegativity[92] and steric effects.[93] Molecular strain in the *syn*- and *anti*-conformers of **M1** originated from the steric hindrance of the voluminous tin-substituents is clearly seen from inspection of the Si–CH_2–Sn angles (Table 5) that are significantly increased (taking as reference the bond angle in an ideal tetrahedron). The Si–CH_2–Sn angles vary from 118.8 to 125.2° for **M1-3$_{SYN}$** and **M1-2$_{ANTI}$** (SB and LB). Similar values were found also for the molecular structure of **BD2** (vide supra).

In contrast to the molecular structure established by SCXRD analysis for building block **BD2**, where the voluminous –SnR_2Cl substituents approximate mutual *anti*-periplanar orientation in relation to the biphenyl connector, in **M1-3$_{SYN}$** and **M1-2$_{ANTI}$** they approach *gauche*-distributions. However, as illustrated by the dihedral angles of the Sn···Si$(CH_3)_2$···Si$(CH_3)_2$···Sn constellations with absolute values in the range from 14.6 to 80.9° for **M1-3$_{SYN}$** (SB and LB) and in the range of 123.1 to 125.5° for **M1-2$_{ANTI}$** (SB and LB), the building block conformations are substantially different in **M1-3$_{SYN}$** and **M1-2$_{ANTI}$**. The differences are reflected also by the torsion angles related to the most

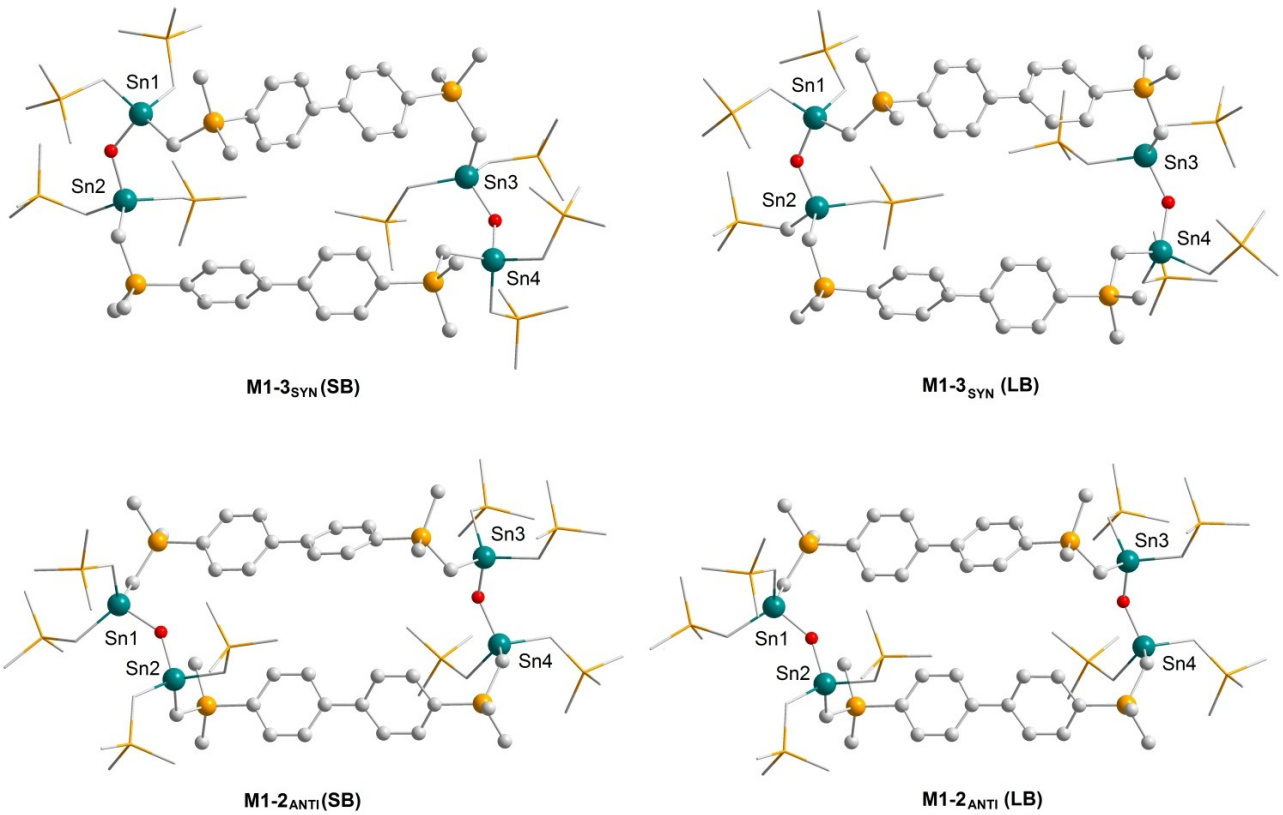

Figure 5. Molecular structures for the conformers **M1-3$_{SYN}$** and **M1-2$_{ANTI}$** calculated at the B3LYP level using a small (SB = def2-svp) and a large (LB = 6-31G*/(Sn)LanL2DZ) basis set.

Table 5. Selected interatomic distances [Å], angles and torsion angles [°] for calculated **M1-3$_{SYN}$** and **M1-2$_{ANTI}$**.[a]

Compound Sn1–O–Sn2 linkage	**M1-3$_{SYN}$ (LB)**	**M1-3$_{SYN}$ (SB)**	**M1-2$_{ANTI}$ (LB)**	**M1-2$_{ANTI}$ (SB)**
Sn–O	1.941	2.014	1.936	2.008
	1.946	2.017	1.935	2.008
Sn–O–Sn	135.0	129.7	146.2	140.4
Sn–CH_2Si_{biph}	2.165	2.195	2.159	2.188
	2.163	2.192	2.162	2.192
Sn–CH_2SiMe_3	2.151	2.181	2.156	2.186
	2.157	2.187	2.164	2.195
	2.151	2.181	2.148	2.177
	2.160	2.191	2.158	2.190
Sn–CH_2–Si_{biph}	120.0	120.4	124.5	125.2
	122.5	120.8	121.8	121.2
Sn–CH_2–$SiMe_3$	119.9	119.3	123.2	123.3
	120.9	121.1	120.8	121.0
	119.8	118.8	122.4	120.8
	121.6	121.1	120.0	119.8
C_{biph}–C_{biph}–Si–CH_2	137.4	134.4	−173.7	171.7
	−119.2	−121.5	63.4	67.4
C_{biph}–Si–CH_2–Sn	−79.8	−71.8	56.7	61.0
	55.1	63.3	57.7	60.4
Si_{biph}–CH_2–Sn–O	161.5	165.5	−92.3	−85.1
	−180.0	−169.6	60.5	58.4
$(CH_2)_{biph}$–Sn–O–Sn	−39.7	−40.7	−132.2	−130.6
	87.0	84.0	90.7	82.8
Sn3–O–Sn4 linkage				
Sn–O	1.942	2.010	1.940	2.013
	1.937	2.010	1.945	2.017
Sn–O–Sn	141.4	139.8	135.3	131.0
Sn–CH_2Si_{biph}	2.158	2.192	2.165	2.193
	2.166	2.193	2.171	2.200
Sn–CH_2SiMe_3	2.152	2.181	2.147	2.179
	2.162	2.190	2.163	2.192
	2.153	2.185	2.146	2.176
	2.156	2.186	2.160	2.188
Sn–CH_2–Si_{biph}	122.8	121.3	124.6	124.7
	119.6	119.8	120.4	120.3
Sn–CH_2–$SiMe_3$	121.7	121.5	120.3	119.0
	122.1	123.8	123.1	122.1
	120.7	119.8	119.8	119.6
	120.7	122.0	122.8	122.3
C_{biph}–C_{biph}–Si–CH_2	−137.4	−179.7	−88.4	−70.3
	139.0	102.9	134.6	133.7
C_{BiPh}–Si–CH_2–Sn	76.9	84.1	84.2	93.4
	−154.1	−154.9	−56.2	−58.5
Si_{biph}–CH_2–Sn–O	−176.6	−167.8	−135.6	−136.5
	−169.4	−175.9	124.5	126.0
$(CH_2)_{biph}$–Sn–O–Sn	87.1	75.8	−76.4	−80.9
	−17.1	2.6	41.0	38.1
Sn···$Si(CH_3)_2$···$Si(CH_3)_2$···Sn	−40.3	−80.9	123.1	124.2
	−14.6	−42.6	−125.5	−123.3

[a] LB (large basis set): 6–31G*/(Sn)LanL2DZ; SB (small basis set): def2-svp.

flexible segments in the building block skeleton, *viz.*, C_{biph}–C_{biph}–Si–CH_2, C_{biph}–Si–CH_2–Sn, Si_{biph}–CH_2–Sn–O and $(CH_2)_{biph}$–Sn–O–Sn (Table 5). On the contrary, the twist of the biphenyl connectors is rather constant in both conformers, with values ranging from 33.1 to 38.2° for **M1-3$_{SYN}$** and **M1-2$_{ANTI}$** (SB/LB) that are slightly smaller than the experimental and calculated value for biphenyl (≈44°).[95] The range of geometric twist variations found for the building block segments within the macrocyclic ring structure of **M1** in its various *syn*- and *anti*-conformers indicates widespread conformational flexibility originated by rotational movements around the C_{biph}–Si, Si–CH_2, CH_2–Sn and Sn–O single bonds, accomplished probably by reorientational motion of the biphenyl spacers, which has been demonstrated to occur in the solid state.[96,97] Because of the small energy difference among **M1-3$_{SYN}$** and **M1-2$_{ANTI}$** (for comparison, the upper limit of weak hydrogen bonds is 4.2 kcal·mol^{-1}),[98] it can be expected that *syn*- and *anti*-conformers of **M1** coexist in solution. Moreover, due to the indications of conformational flexibility a dynamic equilibrium should be expected in solution, which is in agreement with the simplicity of the ^{1}H, ^{13}C, ^{29}Si and ^{119}Sn NMR spectra (note, e.g., the single set of signals for the CH_2– and $Si_{biph}(CH_3)_2$–hydrogen atoms in Figure 3). Dynamic equilibria fast on the NMR time

scales are common in macrocyclic and cage-type assemblies based on organotin complexes.[43,99]

Another set of important parameters in these systems are the transannular Sn···Sn, O···O and Si_{biph}···Si_{biph} distances. The largest difference between **M1-3$_{SYN}$** and **M1-2$_{ANTI}$** are observed for the O···O and Si_{biph}···Si_{biph} distances (Table 6), indicating a closer approximation of the biphenyl moieties in **M1-2$_{ANTI}$**. In a more detailed approach for the determination of the molecular dimensions, spacefilling models were generated for **M1-3$_{SYN}$** (LB) and **M1-2$_{ANTI}$** (LB) (Figure 6). The geometric data listed in Table 6 indicate that the molecular dimensions of the *syn*- and *anti*-conformers are quite similar. The calculated molecular volume of 1465 Å^3 for both **M1-3$_{SYN}$** (LB) and **M1-2$_{ANTI}$** (LB), is in good accordance with the hydrodynamic volume determined experimentally by the DOSY experiment (r_H = 7.5 Å, V_H = 1767 Å^3) in C_6D_6 as solvent (see NMR characterization section). The molecule extensions ($L \times W \times H$), as defined by the generation of a box around the molecular structures of **M1-3$_{SYN}$** (LB) and **M1-2$_{ANTI}$** (LB), are 26.4×13.6×15.5 Å^3 and 27.7×13.3×14.7 Å^3, respectively. However, despite the relatively large molecule size, the molecular structures of **M1$_{SYN}$** and **M1$_{ANTI}$** lack cavities due to intramolecular $Si(CH_3)_3$···$(CH_3)_3Si$ and C–H···π contacts.

Table 6. Data used for the analysis of the molecular dimensions for calculated **M1-3$_{SYN}$** and **M1-2$_{ANTI}$**.[a,b]

	O···O	Si_{biph}···Si_{biph}	Sn···Sn[c]	
M1-3$_{SYN}$ LB	14.583	7.464/7.869	13.410/13.338	
M1-3$_{SYN}$ SB	14.997	7.705/7.007	13.915/13.540	
M1-2$_{ANTI}$ LB	12.445	6.870/6.619	13.949/12.833	
M1-2$_{ANTI}$ SB	12.533	6.622/6.950	14.230/12.985	
	L	*W*	*H*	$V_{molecule}$
M1-3$_{SYN}$ LB	26.4	13.6	15.5	1465
M1-3$_{SYN}$ SB	26.5	13.7	15.6	1472
M1-2$_{ANTI}$ LB	27.7	13.3	14.7	1465
M1-2$_{ANTI}$ SB	27.5	13.6	14.6	1471

[a] LB (large basis set): 6-31G*/(Sn)LanL2DZ; SB (small basis set): def2-svp. [b] Data are reported in Å and Å^3; *L*, *W* and *H* correspond to the length, width and height of a box surrounding the molecular structure, which was calculated by the *wbox* tool implemented in OLEX;[100] $V_{molecule}$ indicates the molecular volume calculated by the *vvol* tool implemented in OLEX.[100] [c] Transannular distance between tin atoms bonded to the same connector.

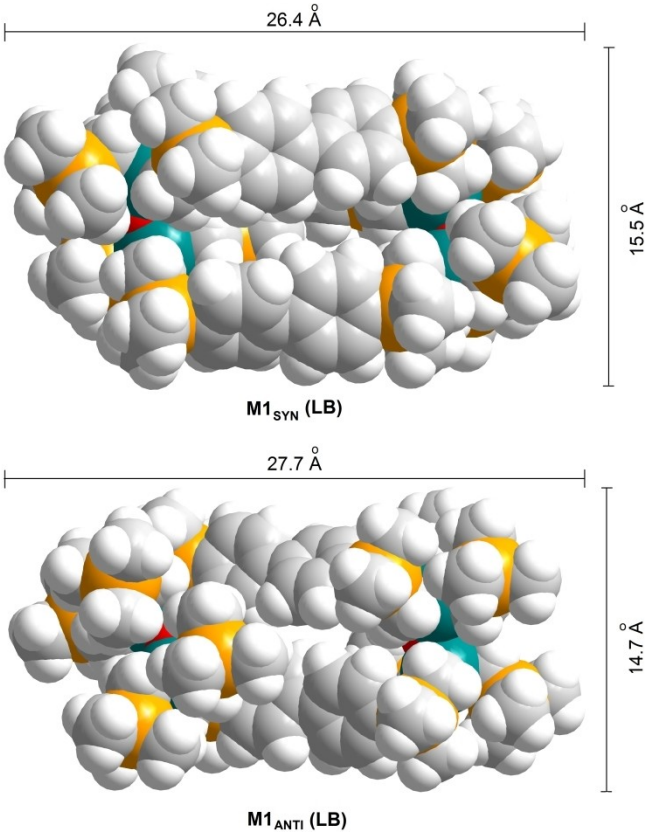

Figure 6. Space filling models of the calculated molecular structures for the conformers **M1-3$_{SYN}$ (LB)** and **M1-2$_{ANTI}$ (LB)**.

Conclusions

A series of six novel di-nuclear organotin compounds, in which the metal atoms are separated by a *p,p'*-biphenylene bridge and carry voluminous $-CH_2Si(CH_3)_3$ and $-CH_2Si(CH_3)_2(C_5H_4FeCp)$ substituents, were synthesized in good overall yields and characterized in detail mainly by NMR spectroscopic methods. In two of the isolated compounds the tin atoms are stereogenic centers, generating characteristic signal splittings in the aliphatic regions of the ^{1}H and ^{13}C NMR spectra. In addition, one of the potential building blocks for metal-directed self-assembly was examined by SCXRD analysis, showing a molecular conformation with mutual *syn*-orientation of the reactive Sn–Cl bonds. This constellation enabled weak intermolecular Cl→Sn interactions to yield a coordination polymer based on tetra-nuclear macrocyclic rings in the solid state. Since the solid-state analysis indicated the suitability of the compounds to function as building blocks for the preparation of macrocycles, the di-nuclear organotin dichloride was reacted with silver (I) oxide to yield, based on Sn–O–Sn linkages, the corresponding [2 + 2] macrocycle. In addition to the spectroscopic and mass spectrometric characterization, the molecular structure and conformations of the 30-membered tetra-nuclear macrocycle **M1** were examined by DFT calculations at the B3LYP/def2svp (small basis set, SB) and B3LYP/6-31G*(C,H,O,Si)/LanL2DZ(Sn) (large basis set, LB) levels of theory. The folded Sn–O–Sn fusion sites and the connecting branches of the organic metal-linkers can be mutually *syn*- or *anti*-oriented, yielding two stereoisomers in the gas phase, named **M1$_{SYN}$** and **M1$_{ANTI}$**. The calculations revealed that **M1$_{SYN}$** is by 2.32(LB)/1.95(SB) kcal·mol^{-1} more stable than **M1$_{ANTI}$**, even though the *anti*-orientation was observed for the macrocyclic dimers [**BD2**]$_2$ in the crystal structure of parent **BD2**. Nevertheless, the small energy difference supports the observation of dynamic equilibria observed by NMR spectroscopy in solution. As determined by the computational calculations, the molecular structures of **M1$_{SYN}$** and **M1$_{ANTI}$** lack cavities due to intramolecular $Si(CH_3)_3$···$(CH_3)_3Si$ and C–H···π contacts.

Interconnection of the tin atoms in the di-nuclear building blocks by ligands other than O^{2-}, e.g., S^{2-}, CO_3^{2-}, $ROPO_3^{2-}$,

SO_4^{2-}, $(O_2C–R–CO_2)^{2-}$, polycarboxylates, and even methylene or oligomethylene dianions, would enable the formation of macrocyclic entities of variable size and Lewis acidity, yielding interesting systems suitable for host-guest chemistry. Moreover, the design of hetero-metallic assemblies can be envisioned as well.

Experimental Section

Synthetic methods and product characterization

Reagents and solvents. *p,p′*-Dibromobiphenyl, chloro (chloromethyl)dimethylsilane, iodine, hydrogen chloride in diethyl ether (2 M solution), *n*-butyllithium, magnesium and silver (I) oxide were acquired from commercial suppliers. $Ph[(CH_3)_3SiCH_2]_2SnI$, $Ph_2[CpFe(C_5H_4Si(CH_3)_2CH_2)]SnI$ and (*p*-$ClCH_2Me_2SiC_6H_4)_2$ (**PRE**) were synthesized according to procedures described in previous reports.[65,101,102] Solvents were dried by standard methods.

Instrumental methods. Elemental analyses were carried out on a Leco CHNS-932 elemental analyzer using samples dried under high vacuum for 6–8 h. Melting points were determined on a Büchi M-560 melting point apparatus and are uncorrected. IR spectra were recorded in the range of 4000–500 cm^{-1} on a Nicolet 6700 FT-IR spectrophotometer using a diamond ATR crystal (compounds **BD1**-**BD4** and **M1**) or a Bruker Tensor-27 equipment using KBr pellets (compounds **BD5** and **BD6**). One-dimensional (^1H, ^{13}C, ^{29}Si, ^{119}Sn) and two-dimensional (COSY, HSQC, HMBC, DOSY) NMR spectroscopic studies were recorded at room temperature on Varian (DRX 200 and Mercury Plus 400), Bruker (Avance III HD 500 and DRX 700) and Jeol (600 MHz) instruments. Standard internal and external references were used: tetramethylsilane ($\delta^1H=0$, $\delta^{13}C=0$ and $\delta^{29}Si=0$) and tetramethylstannane ($\delta^{119}Sn=0$). Mass spectra were recorded on Jeol MStation700 (FAB^+) and Jeol AccuTOF-DART (PaperSpray) spectrometers.

Synthetic procedures

Synthesis of [p-Ph(Me$_3$SiCH$_2$)$_2$SnCH$_2$Me$_2$SiC$_6$H$_4$]$_2$ (BD1)

PRE (1.55 g, 4.22 mmol) and excess Mg (2.05 g, 84.36 mmol) were dissolved in 100 mL of dry THF under nitrogen atmosphere followed by heating at reflux for 6 h. After cooling the solution to room temperature, a solution of $Ph[(CH_3)_3SiCH_2]_2SnI$ (4.19 g, 8.44 mmol) in 20 mL of THF was added dropwise. The mixture was stirred overnight and then hydrolyzed with distilled water. The organic phase was extracted with CH_2Cl_2 and dried over $MgSO_4$. After filtration, the solvent was removed in *in vacuo*. The resulting solid was washed with ethanol and dried under vacuum to yield 3.52 g (3.39 mmol, 80%) of the product. M.p. 77–79 °C. **^{1}H NMR** ($CDCl_3$, 400.2 MHz, 298 K, δ[ppm]): −0.01, 0.00 (s, 44H, H3, H4), 0.30 (s, 12H, H1), 0.32 (s, 4H, H2), 7.29 (m, 6H, H_m, H_p), 7.43 (m, 4H, H_o), 7.57 (AB, 8H, H2′, H3′). **^{13}C NMR** ($CDCl_3$, 100.6 MHz, 298 K, δ[ppm]): −3.1 (C2), −2.2 (C3), 0.6 (C1), 2.1 (C4), 126.8 (C3′), 128.2 (C_m), 128.4 (C_p), 134.2 (C2′), 136.3 (C_o), 140.5 (C1′), 141.9 (C4′), 143.8 (C_i). **^{119}Sn NMR** ($CDCl_3$, 149.2 MHz, 298 K, δ[ppm]): −14. **^{29}Si NMR** ($CDCl_3$, 79.5 MHz, 298 K, δ[ppm]): −2.0, 2.4. **Elemental analysis** calcd. for $C_{46}H_{78}Si_6Sn_2$ (1037.06 $gmol^{-1}$): C, 53.3; H, 7.6%. Found: C, 53.2; H, 7.6%.

Synthesis of [p-Cl(Me$_3$SiCH$_2$)$_2$SnCH$_2$Me$_2$SiC$_6$H$_4$]$_2$ (BD2)

BD1 (1.00 g, 0.96 mmol) and 30 mL of dichloromethane were placed into a 100 mL ball flask equipped with a magnetic stirring bar. The solution was cooled to 0 °C, whereupon 0.96 mL of a 2 M solution of hydrogen chloride in diethyl ether (1.92 mmol) diluted in 30 mL of dichloromethane were added dropwise over a time period of one hour. The mixture was stirred overnight. Subsequently, the solvent was evaporated and the solid dried under vacuum to give the product in form of a yellow solid in 97% yield (0.89 g, 0.93 mmol). Crystals suitable for single-crystal X-ray diffraction analysis were grown by slow solvent evaporation of a solution in $CHCl_3$/MeOH (8:2, *v/v*). M.p. 76–78 °C. **IR** (ν[cm^{-1}]): 526 (m), 529 (m), 588 (m), 645 (m), 693 (s), 715 (s), 764 (s), 776 (s), 801 (s), 827 (s), 1018 (m), 1113 (m), 1247 (s), 1406 (w), 1596 (w), 2894 (w), 2951 (w). ^{1}H NMR ($CDCl_3$, 600.2 MHz, 298 K, δ[ppm]): 0.08 (s, 36H, H4), 0.17 (s, 8H, H3), 0.45 (s, 12H, H1), 0.57 (s, 4H, H2), 7.62 (AB, 8H, H2′, H3′). ^{13}C NMR ($CDCl_3$, 150.9 MHz, 298 K, δ[ppm]): 0.3 (C1), 1.8 (C4), 6.1 (C2), 6.6 (C3), 127.0 (C3′), 134.2 (C2′), 139.4 (C1′), 141.9 (C4′). ^{119}Sn NMR ($CDCl_3$, 223.8 MHz, 298 K, δ[ppm]): 173. **^{29}Si NMR** ($CDCl_3$, 119.2 MHz, 298 K, δ[ppm]): −2.6, 2.3. Elemental analysis calcd. for $C_{34}H_{68}Cl_2Si_6Sn_2$ (953.75 $gmol^{-1}$): C, 42.8; H, 7.2%. Found: C, 43.0; H, 7.0%. **MS** (FAB^+) for $[C_{34}H_{68}ClSi_6Sn_2]^+$ ($[M–Cl]^+$): *m/z* = 917 (92%).

Synthesis of [p-I(Me$_3$SiCH$_2$)$_2$SnCH$_2$Me$_2$SiC$_6$H$_4$]$_2$ (BD3)

BD1 (1.00 g, 0.96 mmol) and 30 mL of dichloromethane were placed into a 100 mL ball flask equipped with a magnetic stirring bar. The solution was cooled to 0 °C, whereupon elemental iodine (0.49 g, 1.93 mmol) was added in small portions during 120 Min. The reaction mixture was stirred overnight. Subsequently, the solvent and the byproduct (iodobenzene) were removed *in vacuo* to give the product as a yellow solid in 98% yield (1.07 g, 0.94 mmol). **IR** (ν[cm^{-1}]): 526 (m), 529 (m), 595 (m), 637 (m), 692 (s), 713 (s), 753 (s), 802 (s), 826 (s), 1002 (m), 1113 (m), 1246 (s), 1301 (w), 1381 (w), 1596 (w), 2950 (w). ^{1}H NMR ($CDCl_3$, 400.2 MHz, 298 K, δ [ppm]): 0.09 (s, 36H, H4), 0.42 (s, 8H, H3), 0.46 (s, 12H, H1), 0.82 (s, 4H, H2), 7.61 (AB, 8H, H2′, H3′). ^{13}C NMR ($CDCl_3$, 100.6 MHz, 298 K, δ[ppm]): 0.4 (C1), 1.9 (C4), 5.3 (C2), 5.8 (C3), 126.9 (C3′), 134.2 (C2′), 139.2 (C1′), 141.9 (C4′). **^{119}Sn NMR** ($CDCl_3$, 149.2 MHz, 298 K, δ [ppm]): 39. ^{29}Si NMR ($CDCl_3$, 79.5 MHz, 298 K, δ[ppm]): −2.1, 2.9. Elemental analysis calcd. for $C_{34}H_{68}I_2Si_6Sn_2$ (1136.66 $gmol^{-1}$): C, 35.9; H, 6.0%. Found: C, 36.1; H, 6.1%.

Synthesis of [p-Ph$_2$(CpFeC$_5$H$_4$SiMe$_2$CH$_2$)SnCH$_2$Me$_2$SiC$_6$H$_4$]$_2$ (BD4)

PRE (1.41 g, 3.84 mmol) and excess Mg (1.87 g, 76.95 mmol) were dissolved in 100 mL of dry THF under nitrogen atmosphere. The mixture was heated at reflux for 6 h. After cooling to room temperature, a solution of $Ph_2[CpFe(C_5H_4Si(CH_3)_2CH_2)]SnI$ (5.04 g, 7.67 mmol) in 20 mL of dry THF was added dropwise. The mixture was stirred overnight and then hydrolyzed with distilled water. The organic phase was extracted with CH_2Cl_2 and dried over $MgSO_4$. After filtration, the solvent was removed under reduced pressure and the remaining solid purified by column chromatography using as eluent a solvent mixture of hexane and diethyl ether (20:1, *v/v*). Subsequent removal of the solvent under reduced pressure yielded the final product in 73% yield (3.80 g, 2.80 mmol). M.p. 47–50 °C. **IR** (ν[cm^{-1}]): 529 (m), 584 (m), 656 (m), 697 (s), 725 (s), 768 (s), 800 (s), 830 (m), 895 (w), 997 (m), 1023 (w), 1034 (w), 1074 (w), 1113 (m), 1162 (m), 1246 (m), 1299 (w), 1380 (w), 1428 (w), 1480 (w), 1595 (w), 2951 (w), 3013 (w), 3062 (w). **^{1}H NMR** ($CDCl_3$, 400.2 MHz, 298 K, δ[ppm]): 0.14 and 0.19 (s, 24H, H1, H4), 0.31 and 0.41 (s, 8H, H2, H3), 4.00 (s, 4H, H2″), 4.08 (s, 10H, H4″), 4.30 (s, 4H, H3″), 7.33 (m, 12H, H_m, H_p), 7.42 (m, 8H, H_o), 7.51 (AB, 8H, H2′, H3′). **^{13}C NMR** ($CDCl_3$, 100.6 MHz, 298 K, δ[ppm]): −4.3 and −2.9 (C2, C3), 0.4 and 1.0 (C1,

C4), 68.4 (C4′′), 71.0 (C3′′), 73.3 (C2′′), 73.5 (C1′′), 126.7 (C3′), 128.5 (C_m), 128.8 (C_p), 134.2 (C2′), 137.0 (C_o), 140.3 (C1′), 141.6 (C_i), 141.8 (C4′). **^{119}Sn NMR** ($CDCl_3$, 149.2 MHz, 298 K, δ[ppm]): −51. **^{29}Si NMR** ($CDCl_3$, 79.5 MHz, 298 K, δ[ppm]): −1.8, −1.3. **Elemental analysis** calcd. for $C_{68}H_{78}Fe_2Si_4Sn_2$ (1356.82 gmol^{-1}): C, 60.2; H, 5.8%. Found: C, 60.5; H, 6.1%. **MS** (FAB$^+$) for $[C_{68}H_{78}Fe_2Si_4Sn_2]^+$ ([M]$^+$): m/z = 1356 (83%).

Synthesis of [p-ClPh(CpFeC$_5$H$_4$SiMe$_2$CH$_2$)SnCH$_2$Me$_2$SiC$_6$H$_4$]$_2$ (BD5)

BD4 (1.00 g, 0.74 mmol) and 30 mL of dichloromethane were placed into a 100 mL ball flask equipped with a magnetic stirring bar. The solution was cooled to 0 °C, whereupon 0.74 mL of a 2 M solution of hydrogen chloride in diethyl ether (1.48 mmol) diluted in 30 mL of dichloromethane were added dropwise over a time period of one hour. The mixture was stirred overnight. Subsequently, the solvent was evaporated and the solid dried under vacuum to give the product in form of a yellow solid in 96% yield (0.91 g, 0.71 mmol). M.p. 50–52 °C. **IR** (ν[cm^{-1}]): 498 (w), 715 (m), 807 (s), 1020 (m), 1108 (m), 1162 (w), 1253 (s), 1594 (m), 1660 (m), 1715 (m), 1758 (w), 2852 (m), 2923 (m), 2962 (m). **^{1}H NMR** ($CDCl_3$, 600.6 MHz, 298 K, δ[ppm]): 0.27–0.37 (m, 24H, H1, H4), 0.49–0.59 (m, 8H, H2, H3), 3.99 (s, 4H, H2′′), 4.10 (s, 10H, H4′′), 4.33 (s, 4H, H3′′), 7.37 (m, 10H, H_o, H_m, H_p), 7.54 (AB, 8H, H2′, H3′). **^{13}C NMR** ($CDCl_3$, 150.9 MHz, 298 K, δ[ppm]): 0.0, 0.3, 0.7 and 0.8 (C1, C4), 3.9 and 5.3 (C2, C3), 68.6 (C4′′), 71.4 (C3′′), 72.0 (C1′′), 73.4 (C2′′), 126.9 (C3′), 128.9 (C_m), 129.9 (C_p), 134.3 (C2′), 135.3 (C_o), 139.2 (C1′), 142.0 (C4′), 142.4 (C_i). **^{119}Sn NMR** ($CDCl_3$, 223.8 MHz, 298 K, δ[ppm]): 98. ^{29}Si NMR ($CDCl_3$, 119.2 MHz, 298 K, δ[ppm]): −2.5, −2.0. Elemental analysis calcd. for $C_{56}H_{68}Cl_2Fe_2Si_4Sn_2$ (1273.51 gmol^{-1}): C, 52.8; H, 5.4%. Found: C, 54.7; H, 5.5%.

Synthesis of [p-IPh(CpFeC$_5$H$_4$SiMe$_2$CH$_2$)SnCH$_2$Me$_2$SiC$_6$H$_4$]$_2$ (BD6)

BD4 (1.00 g, 0.74 mmol) and 30 mL of dichloromethane were placed into a 100 mL ball flask equipped with a magnetic stirring bar. The solution was cooled to 0 °C, whereupon iodine (0.37 g, 1.47 mmol) was added in small portions during 120 Min. The reaction mixture was allowed to stir overnight. Subsequently, the solvent and the byproduct (iodobenzene) were removed in vacuo to give the product as a yellow solid in 97% yield (1.05 g, 0.72 mmol). **IR** (ν[cm^{-1}]): 445 (w), 501 (w), 597 (w), 657 (w), 696 (m), 727 (s), 774 (s), 806 (s), 895 (w), 1002 (s), 1112 (m), 1162 (m), 1250 (s), 1299 (w), 1382 (w), 1428 (w), 1481 (w), 1529 (w), 1596 (w), 1632 (w), 2955 (m), 3013 (w), 3065 (w). **^{1}H NMR** ($CDCl_3$, 400.2 MHz, 298 K, δ[ppm]): 0.28–0.39 (m, 24H, H1, H4), 0.73–0.81 (m, 8H, H2, H3), 4.00 (s, 4H, H2′′), 4.12 (s, 10H, H4′′), 4.34 (s, 4H, H3′′), 7.34 (m, 6H, H_m, H_p), 7.43 (m, 4H, H_o), 7.56 (AB, 8H, H2′, H3′). **^{13}C NMR** ($CDCl_3$, 100.6 MHz, 298 K, δ[ppm]): 0.1, 0.3, 0.7 and 0.9 (C1, C4), 3.4 and 4.9 (C2, C3), 68.5 (C4′′), 71.3 (C3′′), 72.0 (C1′′), 73.5 (C2′′), 126.8 (C3′), 128.7 (C_m), 129.7 (C_p), 134.3 (C2′), 135.6 (C_o), 139.2 (C1′), 140.2 (C_i), 141.9 (C4′). **^{119}Sn NMR** ($CDCl_3$, 223.8 MHz, 298 K, δ[ppm]): −13. ^{29}Si NMR ($CDCl_3$, 119.2 MHz, 298 K, δ[ppm]): −2.0, −1.5. **MS** (FAB$^+$) for $[C_{56}H_{68}Fe_2I_2Si_4Sn_2]^+$ ([M]$^+$): m/z = 1457 (35%).

Synthesis of the [2 + 2] macrocycle M1

A solution of **BD2** (0.60 g, 0.63 mmol) in 50 mL of CH_2Cl_2 was placed into a 100 mL ball flask equipped with a magnetic stirring bar, whereupon solid silver oxide (0.15 g, 0.63 mmol) was added. The reaction mixture was stirred overnight and then filtered to remove AgCl. The solvent was removed and the solid dried in vacuum to give the product in form of a colorless solid in 89% yield (0.51 g, 0.28 mmol). M.p. 101–103 °C. **IR** (ν[cm^{-1}]): 526 (m), 529 (m), 533 (m), 591 (m), 637 (m), 693 (s), 712 (s), 752 (s), 802 (s), 826 (s), 1002 (m), 1114 (m), 1245 (m), 1404 (w), 1597 (w), 2892 (w), 2950 (w). **^{1}H NMR** ($CDCl_3$, 199.9 MHz, 298 K, δ[ppm]): −0.01 (s, 16H, H3), 0.05 (s, 72H, H4), 0.35 (s, 8H, H2), 0.41 (s, 24H, H1), 7.60 (AB, 16H, H2′, H3′). **^{13}C NMR** ($CDCl_3$, 50.2 MHz, 298 K, δ [ppm]: 0.5 (C1), 1.9 (C4), 3.9 (C2), 4.6 (C3), 127.0 (C3′), 134.2 (C2′), 139.9 (C1′), 142.1 (C4′). **^{119}Sn NMR** ($CDCl_3$, 186.4 MHz, 298 K, δ [ppm]): 133. **^{29}Si NMR** ($CDCl_3$, 99.3 MHz, 298 K, δ[ppm]): −2.9, 1.6. **HR-MS** (PaperSpray) for $[C_{68}H_{137}O_2Si_{12}Sn_4]^+$ ([M + H]$^+$): m/z = 1797.39807 (mmu −3.01, 29%).

Single-crystal X-ray diffraction analysis

Intensity data for a crystal of compound **BD2** were collected at T = 298 K on a Bruker Venture diffractometer equipped with an area detector using Mo-K_α radiation (λ = 0.71073 Å). For the data collection, the Bruker APEX3 software was used. The measured intensities were reduced to F^2 using SAINT and corrected for absorption effects by the multi-scan method (SADABS). Structure solution, refinement, and data output were performed with the OLEX2[100] program package using SHELXT[103] for the structure solution and SHELXL[104] for the refinement. Non-hydrogen atoms were refined anisotropically. All C–H hydrogen atoms were placed in geometrically calculated positions using the riding model.

The crystals diffracted weakly and were twinned (two-component twin). In addition, the asymmetric unit contains only half the molecule due to crystallographic symmetry (2-axis). The $-CH_2SiMe_3$ substituents attached to the tin atoms exhibit disorder over two positions. The disordered groups were refined using geometry and U_{ij} restraints.

Figures were created with Diamond.[105] Table S7 summarizes the most relevant crystallographic data (see ESI).

Theoretical calculations

Quantum chemical calculations for the macrocyclic compound **M1** in form of *syn*- (**M1$_{SYN}$**) and *anti*-conformers (**M1$_{ANTI}$**) were performed to obtain the geometry-optimized minimum energy structures with 1×10^{-8} convergence requested. All calculations were developed with the Northwest Computational Chemistry Package (NWChem) version 6.8,[86] using the B3LYP hybrid functional[80,81] in combination with the def2-svp[82] (small basis, SB) and 6–31G*/LanL2DZ (large basis, LB)[83,84] basis sets.[85] Both basis set combinations are recommended for the consideration of relativistic effects as well as accounting for effective core potentials (ECP) for the heavy atom (Sn) present in **M1**.

Deposition Number 2068068 (for **BD2**) contains the supplementary crystallographic data for this paper. These data are provided free of charge by the joint Cambridge Crystallographic Data Centre and Fachinformationszentrum Karlsruhe Access Structures service www.ccdc.cam.ac.uk/structures.

Supporting Information (see footnote on the first page of this article): NMR, IR and mass spectra for **BD1**–**BD6** and **M1** (Figures S1–S42). Tables with a comparative overview of ^{1}H, ^{13}C, ^{29}Si and ^{119}Sn NMR data for **BD1**–**BD6** and **M1** (Tables S1–S6), crystallographic data for **BD2** (Table S7) and bond angles for the tin atoms in the calculated structures of **M1-3$_{SYN}$** and **M1-2$_{ANTI}$** (Tables S8).

Acknowledgements

This work received support from Consejo Nacional de Ciencia y Tecnologia (CONACyT), Mexico and Consejo Mexiquense de Ciencia y Tecnologia (COMECyT) in form of postgraduate fellow-

*ships for GGJ and IRL. Financial support from CONACyT through project numbers 158098 and 229929 is gratefully acknowledged. Access to Laboratorio Nacional de Estructura de Macromoléculas (LANEM) and technical assistance from Ing. Victoria Labastida Galván, Dr. Perla Román Bravo and Dr. Gabriela Vargas Pineda are acknowledged. We thank Dra. Rosa Santillan at CINVESTAV-IPN Mexico and Dr. Robert B. Cody from Jeol USA, Inc., for the detailed mass spectrometric determination of the [2+2] macrocycle **M1** using different techniques (electrospray, paperspray and DART), and Dr. Rubén A. Toscano from Instituto de Química, Universidad Nacional Autónoma de México (IQ-UNAM) for the collection of X-ray diffraction data. HIB thanks CONACyT (grant 243224) and UAM for research funding as well as UAM-Iztapalapa for access and support to the Yoltla cluster supercomputing facilities. Open access funding enabled and organized by Projekt DEAL.*

Conflict of Interest

The authors declare no conflict of interest.

Keywords: Organotin compounds · Metalla-macrocyclic chemistry · DOSY NMR spectroscopy · X-ray diffraction analysis · Self-assembly with dinuclear building block (tecton)

[1] T. Gajda, A. Jancsó in *Metal Ions in Life Sciencies*, Vol. 7 (Eds.: A. Sigel, H. Sigel, R. K.O. Sigel), Royal Society of Chemistry, United Kingdom, **2010**, pp. 111–151.
[2] H. Zimmer, H. G. Moslé, *Chem. Ber.* **1954**, *87*, 1255–1257.
[3] S. D. Rosenberg, E. Debreczeni, E. L. Weinberg, *J. Am. Chem. Soc.* **1959**, *81*, 972–975.
[4] I. L. Marr, D. Rosales, J. L. Wardell, *J. Organomet. Chem.* **1988**, *349*, 65–74.
[5] M. Gielen, *Acc. Chem. Res.* **1973**, *6*, 198–202, and references therein.
[6] M. G. Voronkov, K. A. Abzaeva in *The Chemistry of Organic Germanium, Tin and Lead Compounds*, Vol. 2 (Ed.: Z. Rappoport), John Wiley & Sons, Chichester, United Kingdom, **2002**, pp. 1–147.
[7] K. Jurkschat, F. Hesselbarth, M. Dargatz, J. Lehmann, E. Kleinpeter, A. Tzschach, J. Meunier-Piret, *J. Organomet. Chem.* **1990**, *388*, 259–271, and references therein.
[8] V. Chandrasekhar, P. Singh, K. Gopal, in *Tin Chemistry: Fundamentals, Frontiers and Applications*, Vol. 2 (Eds.: M. Gielen, A. Davies, K. Pannell, E. Tiekink), John Wiley & Sons, Chichester, United Kingdom, **2008**, pp. 93–116, and references therein.
[9] H. Höpfl, in *Tin Chemistry: Fundamentals, Frontiers and Applications*, Vol. 2 (Eds.: M. Gielen, A. Davies, K. Pannell, E. Tiekink), John Wiley & Sons, Chichester, United Kingdom, **2008**, pp. 117–137, and references therein.
[10] M. Newcomb, Y. Azuma, A. R. Courtney, *Organometallics* **1983**, *2*, 175–177.
[11] J. Ayari, C. R. Göb, I. M. Oppel, M. Lutter, W. Hiller, K. Jurkschat, *Angew. Chem. Int. Ed.* **2020**, *59*, 23892–23898; *Angew. Chem.* **2020**, *132*, 24102–24109.
[12] A. Torres-Huerta, J. Cruz-Huerta, H. Höpfl, L. G. Hernandez-Vazquez, J. Escalante-Garcia, A. Jimenez-Sanchez, R. Santillan, I. F. Hernandez-Ahuactzi, M. Sanchez, *Inorg. Chem.* **2016**, *55*, 12451–12469.
[13] M. R. Halvagar, Z. Hassanzadeh Fard, S. Dehnen, *Chem. Eur. J.* **2011**, *17*, 4371–4374.
[14] M. Newcomb, M. T. Blanda, Y. Azuma, T. J. Delord, *J. Chem. Soc. Chem. Commun.* **1984**, *17*, 1159–1160.
[15] B. Ruan, Y. Tian, H. Zhou, J. Wu, R. Hu, C. Zhu, J. Yang, H. Zhu, *Inorg. Chim. Acta* **2011**, *365*, 302–308.
[16] V. Chandrasekhar, P. Thilagar, J. F. Bickley, A. Steiner, *J. Am. Chem. Soc.* **2005**, *127*, 11556–11557.
[17] M. Mehring, I. Paulus, B. Zobel, M. Schürmann, K. Jurkschat, A. Duthie, D. Dakternieks, Eur. J. Inorg. Chem. 2001, 153–160.
[18] Z. Hassanzadeh Fard, M. R. Halvagar, S. Dehnen, *J. Am. Chem. Soc.* **2010**, *132*, 2848–2849.
[19] C. Ma, Q. Zhang, R. Zhang, D. Wang, *Chem. Eur. J.* **2006**, *12*, 420–428.
[20] R.-H. Wang, M.-C. Hong, J.-H. Luo, R. Cao, J.-B. Weng, *Eur. J. Inorg. Chem.* **2008**, *47*, 2082–2085.
[21] R. García-Zarracino, H. Höpfl, M. Güizado-Rodríguez, *Cryst. Growth Des.* **2009**, *9*, 1651–1654.
[22] V. Chandrasekhar, C. Mohapatra, R. J. Butcher, *Cryst. Growth Des.* **2012**, *12*, 3285–3295.
[23] C. Mohapatra, V. Chandrasekhar, *Cryst. Growth Des.* **2014**, *14*, 406–409.
[24] D. Dakternieks, A. Duthie, B. Zobel, K. Jurkschat, M. Schürmann, E. R. T. Tiekink, *Organometallics* **2002**, *21*, 647–652.
[25] R. Reyes-Martínez, P. García y García, M. López-Cardoso, H. Höpfl, H. Tlahuext, *Dalton Trans.* **2008**, 6624–6627.
[26] I. F. Hernández-Ahuactzi, J. Cruz-Huerta, H. Tlahuext, V. Barba, J. Guerrero-Alvarez, H. Höpfl, *Cryst. Growth Des.* **2015**, *15*, 829–847.
[27] M. G. Vasquez-Ríos, I. Rojas-León, P. Montes-Tolentino, I. F. Hernández-Ahuactzi, H. Höpfl, *Cryst. Growth Des.* **2018**, *18*, 7132–7149.
[28] K. Jurkschat, N. Pieper, S. Seemeyer, M. Schürmann, M. Biesemans, I. Verbruggen, R. Willem, *Organometallics* **2001**, *20*, 868–880.
[29] J. Otera, M. Biesemans, V. Pinoie, K. Poelmans, R. Willem in *Tin Chemistry: Fundamentals, Frontiers and Applications*, Vol. 2 (Eds.: M. Gielen, A. Davies, K. Pannell, E. Tiekink), John Wiley & Sons, Chichester, United Kingdom, **2008**, pp. 312–323, and references therein.
[30] Pablo Espinet, M. Genov in *Tin Chemistry: Fundamentals, Frontiers and Applications*, Vol. 2 (Eds.: M. Gielen, A. Davies, K. Pannell, E. Tiekink), John Wiley & Sons, Chichester, United Kingdom, **2008**, pp. 561–578, and references therein.
[31] M. T. Blanda, J. H. Horner, M. Newcomb, *J. Org. Chem.* **1989**, *54*, 4626–4636.
[32] M. G. Vasquez-Ríos, V. Reyes-Márquez, H. Höpfl, A. Torres-Huerta, J. Guerrero-Álvarez, M. Sánchez, I. F. Hernández-Ahuactzi, K. Ochoa-Lara, A. Jiménez-Sánchez, R. Santillán, *Eur. J. Inorg. Chem.* **2016**, *2016*, 3429–3440.
[33] M. M. Naseer, K. Jurkschat, *Chem. Commun.* **2017**, *53*, 8122–8135.
[34] Á. Y. Castrejón-Antúnez, M. Mendoza-Mendoza, D. I. Olea-López, F. Medrano, H. Tlahuext, J. Guerrero-Álvarez, G. Vargas-Pineda, C. Godoy-Alcántar, *Polyhedron* **2016**, *111*, 132–142.
[35] R. Yadav, M. Kumar Awasthi, A. Singh, G. Kociok-Köhn, M. Trivedi, R. Prasad, M. Shahid, A. Kumar, *J. Mol. Struct.* **2017**, *1145*, 197–203.
[36] P. Lacroix, N. Farfán in *Tin Chemistry: Fundamentals, Frontiers and Applications*, Vol. 2 (Eds.: M. Gielen, A. Davies, K. Pannell, E. Tiekink), John Wiley & Sons, Chichester, United Kingdom, **2008**, pp. 351–360, and references therein.
[37] J. A. Lara-Cerón, V. M. Jiménez-Pérez, A. A. Molina-Paredes, M. E. Ochoa, R. M. Sábio, A. C. Amaral, R. R. da Silva, S. J. L. Ribeiro, H. da S. Barud, B. M. Muñoz-Flores, *Inorg. Chim. Acta* **2020**, *505*, 119490.
[38] H. K. Sharma, K. H. Pannell in *Tin Chemistry: Fundamentals, Frontiers and Applications*, Vol. 2 (Eds.: M. Gielen, A. Davies, K. Pannell, E. Tiekink), John Wiley & Sons, Chichester, United Kingdom, **2008**, pp. 376–391, and references therein.
[39] S. K. Hadjikakou, N. Hadjiliadis, *Coord. Chem. Rev.* **2009**, *253*, 235–249.
[40] C. Pellerito, L. Nagy, L. Pellerito, A. Szorcsik, *J. Organomet. Chem.* **2006**, *691*, 1733–1747.
[41] J. C. Berrones-Reyes, B. M. Muñoz-Flores, A. C. Uscanga-Palomeque, R. Santillán, C. Del Angel-Mosqueda, D. Nobis, M. A. Cochrane, S. W. Magennis, V. M. Jiménez-Pérez, *ChemistrySelect* **2020**, *5*, 1623–1627.
[42] T. S. Basu Baul, M. Rao Addepalli, A. Duthie, P. Singh, B. Koch, H. Gildenast, U. Englert, I. Rojas-León, H. Höpfl, *Appl. Organomet. Chem.* **2020**, *35*, e6080.
[43] R. García-Zarracino, J. Ramos-Quiñones, H. Höpfl, *Inorg. Chem.* **2003**, *42*, 3835–3845.
[44] C. Ma, Y. Han, R. Zhang, D. Wang, *Dalton Trans.* **2004**, 1832–1840.
[45] G. Prabusankar, R. Murugavel, *Organometallics* **2004**, *23*, 5644–5647.
[46] T. S. Basu Baul, K. S. Singh, A. Lyčka, M. Holčapek, A. Linden, *J. Organomet. Chem.* **2005**, *690*, 1581–1587.
[47] C. Ma, Q. Zhang, R. Zhang, D. Wang, *Chem. Eur. J.* **2006**, *12*, 420–428.
[48] V. Chandrasekhar, R. Thirumoorthi, *Organometallics* **2007**, *26*, 5415–5422.
[49] T. S. Basu Baul, D. Dutta, A. Duthie, M. F. C. Guedes da Silva, *Inorg. Chem. Commun.* **2017**, *84*, 68–71.
[50] Y.-P. Xie, J.-F. Ma, J. Yang, M.-Z. Su, *Dalton Trans.* **2010**, *39*, 1568–1575.

[51] N. A. Celis, R. Villamil-Ramos, H. Höpfl, I. F. Hernández-Ahuactzi, M. Sánchez, L. S. Zamudio-Rivera, V. Barba, *Eur. J. Inorg. Chem.* **2013**, *2013*, 2912–2922.
[52] C. A. Kraus, H. Eatough, *J. Am. Chem. Soc.* **1933**, *55*, 5014–5016.
[53] Z. You, K. Harms, S. Dehnen, *Eur. J. Inorg. Chem.* **2015**, 5322–5328.
[54] K. Hanau, N. Rinn, M. Argentari, S. Dehnen, *Chem. Eur. J.* **2018**, *24*, 11711–11716.
[55] P. Brunet, M. Simard, J. D. Wuest, *J. Am. Chem. Soc.* **1997**, *119*, 2737–2738.
[56] M. W. Hosseini, *Acc. Chem. Res.* **2005**, *38*, 313–323.
[57] M. Mehring, M. Schürmann, H. Reuter, D. Dakternieks, K. Jurkschat, *Angew. Chem. Int. Ed. Engl.* **1997**, *36*, 1112–1114.
[58] B. Zobel, M. Schürmann, K. Jurkschat, D. Dakternieks, A. Duthie, *Organometallics* **1998**, *17*, 4096–4104.
[59] R. Altmann, O. Gausset, D. Horn, K. Jurkschat, M. Schürmann, M. Fontani, P. Zanello, *Organometallics* **2000**, *19*, 430–443.
[60] H. Elhamzaoui, B. Jousseaume, H. Riague, T. Toupance, P. Dieudonné, C. Zakri, M. Maugey, H. Allouchi, *J. Am. Chem. Soc.* **2004**, *126*, 8130–8131.
[61] H. Elhamzaoui, B. Jousseaume, T. Toupance, C. Zakri, M. Biesemans, R. Willem, H. Allouchi, *Chem. Commun.* **2006**, 1304–1306.
[62] T. Toupance, H. El Hamzaoui, B. Jousseaume, H. Riague, I. Saadeddin, G. Campet, J. Brötz, *Chem. Mater.* **2006**, *18*, 6364–6372.
[63] T. Toupance, M. de Borniol, H. El Hamzaoui, B. Jousseaume, *Appl. Organomet. Chem.* **2007**, *21*, 514–520.
[64] P. Vasko, S. Wang, H. M. Tounonen, P. P. Power, *Angew. Chem.* **2015**, *127*, 3873–3876; *Angew. Chem. Int. Ed.* **2015**, *54*, 3802–3805.
[65] I. Rojas-Leon, H. Alnasr, K. Jurkschat, M. G. Vasquez-Rios, I. F. Hernandez-Ahuactzi, H. Höpfl, *Chem. Eur. J.* **2018**, *24*, 4547–4551.
[66] I. Rojas-León, H. Alnasr, K. Jurkschat, M. G. Vasquez-Ríos, G. Gómez-Jaimes, H. Höpfl, I. F. Hernández-Ahuactzí, R. Santillan, *Organometallics* **2019**, *38*, 2443–2460.
[67] I. Rojas-León, M. G. Hernández-Cruz, E. C. Vargas-Olvera, H. Höpfl, H. Alnasr, K. Jurkschat, *J. Organomet. Chem.* **2020**, *920*, 121344.
[68] V. Chandrasekhar, S. Nagendran, V. Baskar, *Coord. Chem. Rev.* **2002**, *235*, 1–52.
[69] B. Wrackmeyer, *Ann. Rep. NMR Spectrosc.* **1985**, *16*, 73–186.
[70] S. S. Batsanov, *Inorg. Mater.* **2001**, *37*, 871–885.
[71] P. Apodaca, F. Cervantes-Lee, K. H. Pannell, *Main Group Met. Chem.* **2001**, *24*, 597–601.
[72] R. A. Varga, K. Jurkschat, C. Silvestru, *Eur. J. Inorg. Chem.* **2008**, 708–716.
[73] S. K. Thodupunoori, I. A. Alamudun, F. Cervantes-Lee, F. D. Gomez, Y. P. Carrasco, K. H. Pannell, *J. Organomet. Chem.* **2006**, *691*, 1790–1796.
[74] M. A. Buntine, F. J. Kosovel, E. R. T. Tiekink, *CrystEngComm.* **2003**, *5*, 331–336.
[75] W. Li, G. Kagan, R. Hopson, P. G. Williard, *J. Chem. Educ.* **2011**, *88*, 1331–1335.
[76] R. Evans, Z. Deng, A. K. Rogerson, A. S. McLachlan, J. J. Richards, M. Nilsson, G. A. Morris, *Angew. Chem. Int. Ed. Engl.* **2013**, *52*, 3199–3202.
[77] D. B. Chambers, F. Glockling, M. Weston, *J. Chem. Soc. A* **1967** 1759–1769.
[78] L. Frish, S. E. Matthews, V. Böhmer, Y. Cohen, *J. Chem. Soc., Perkin Trans. 2* **1999**, 669–672.
[79] R. B. Cody, T. Fouquet, *J. Am. Soc. Mass Spectrom.* **2019**, *30*, 1321–1324.
[80] A. D. Becke, *J. Chem. Phys.* **1993**, *98*, 5648–5652.
[81] C. Lee, W. Yang, R. G. Parr, *Phys. Rev.* **1988**, *B37*, 785–789.
[82] F. Weigend, R. Ahlrichs, *Phys. Chem. Chem. Phys.* **2005**, *7*, 3297–3305.
[83] P. C. Hariharan, J. A. Pople, *Theor. Chim. Acta* **1973**, *28*, 213–222.
[84] W. R. Wadt, P. J. Hay, *J. Chem. Phys.* **1985**, *82*, 284–298.
[85] B. P. Pritchard, D. Altarawy, B. Didier, T. D. Gibson, T. L. Windus, *J. Chem. Inf. Model.* **2019**, *59*, 4814–4820.
[86] M. Valiev, E. J. Bylaska, N. Govind, K. Kowalski, T. P. Straatsma, H. J. J. Van Dam, D. Wang, J. Nieplocha, E. Apra, T. L. Windus, W. A. de Jong, *Comp. Phys. Commun.* **2010**, *181*, 1477–1489.
[87] M. A. Buntine, V. J. Hall, F. J. Kosovel, E. R. T. Tiekink, *J. Phys. Chem. A* **1998**, *102*, 2472–2482.
[88] M. Naseh, T. Sedaghat, A. Tarassoli, E. Shakerzadeh, *Comp. Theor. Chem.* **2013**, *1005*, 53–57.
[89] K. Gholivand, M. Rajabi, N. Dorosti, F. Molaei, *Appl. Organomet. Chem.* **2015**, *29*, 739–745.
[90] R. Kadu, H. Roy, V. K. Singh, *Appl. Organomet. Chem.* **2015**, *29*, 746–755.
[91] C. Glidewell, D. C. Liles, *Acta Crystallogr. Sect. B* **1978**, *34*, 1693–1695.
[92] C. Glidewell, D. C. Liles, *Acta Crystallogr. Sect. B* **1979**, *35*, 1689–1691.
[93] S. Kerschl, B. Wrackmeyer, D. Männig, H. Nöth, R. Staudigl, *Z. Naturforsch. B* **1987**, *42*, 387–394.
[94] Y.-Q. Huang, Z.-G. Zhang, Q.-L. Xie, *Phosphorus, Sulfur, and Silicon and the Related Elements* **2002**, *177*, 1271–1279.
[95] M. P. Johansson, J. Olsen, *J. Chem. Theory Comput.* **2008**, *4*, 1460–1471.
[96] A. Fujiwara, Y. Inagaki, H. Momma, E. Kwon, K. Yamaguchi, M. Kanno, H. Kono, W. Setaka, *CrystEngComm* **2017**, *19*, 6049–6056.
[97] Z. J. O'Brien, S. D. Karlen, S. Khan, M. A. Garcia-Garibay, *J. Org. Chem.* **2010**, *75*, 2482–2491.
[98] E. Arunan, G. R. Desiraju, R. A. Klein, J. Sadlej, S. Scheiner, I. Alkorta, D. C. Clary, R. H. Crabtree, J. J. Dannenberg, P. Hobza, H. G. Kjaergaard, A. C. Legon, B. Mennucci, D. J. Nesbitt, *Pure Appl. Chem.* **2011**, *83*, 1637–1641.
[99] I. F. Hernández-Ahuactzi, J. Cruz-Huerta, V. Barba, H. Höpfl, L. S. Zamudio-Rivera, H. I. Beltrán, *Eur. J. Inorg. Chem.* **2008**, *8*, 1200–1204.
[100] O. V. Dolomanov, L. J. Bourhis, R. J. Gildea, J. A. K. Howard, H. Puschmann, *J. Appl. Crystallogr.* **2009**, *42*, 339–341.
[101] X. Kong, T. B. Grindley, P. K. Bakshi, T. S. Cameron, *Organometallics* **1993**, *12*, 4881–4886.
[102] R. Altmann, M. Fontani, O. Gausset, K. Jurkschat, M. Schürmann, P. Zanello, *Phosphorus, Sulfur and Silicon* **1999**, *150–151*, 299–304.
[103] G. Sheldrick, *Acta Crystallogr. Sect. A* **2015**, *71*, 3–8.
[104] G. Sheldrick, *Acta Crystallogr. Sect. C* **2015**, *71*, 3–8.
[105] K. Brandenburg, Diamond v3.2e, Crystal Impact, Bonn (Germany), **2010**.

Manuscript received: March 4, 2021
Revised manuscript received: April 23, 2021
Accepted manuscript online: April 30, 2021